Chinese Chemical Letters 35 (2024) 109257

Contents lists available at ScienceDirect

Chinese Chemical Letters

journal homepage: www.elsevier.com/locate/cclet

# Recent advances in heterogeneous hydrosilylation of unsaturated carbon-carbon bonds

Heng Yang[a], Zhijie Zhou[a], Conghui Tang[b,*], Feng Chen[a,*]

[a] School of Chemistry and Chemical Engineering, Yangzhou University, Yangzhou 225002, China
[b] Key Laboratory of Material Chemistry for Energy Conversion and Storage, Ministry of Education, Hubei Key Laboratory of Material Chemistry and Service Failure, School of Chemistry and Chemical Engineering, Huazhong University of Science and Technology, Wuhan 430074, China

ARTICLE INFO

*Article history:*
Received 3 August 2023
Revised 19 October 2023
Accepted 27 October 2023
Available online 30 October 2023

*Keywords:*
Hydrosilylation
Heterogeneous catalysis
Alkenes
Alkynes
Silanes

ABSTRACT

The hydrosilylation of unsaturated carbon-carbon bonds is one of the most critical reactions in silicone industrial production. The homogeneous Speier's catalyst, Karstedt's catalyst, and other noble metal-based catalysts are widely used. However, simplifying the separation of the homogeneous catalyst from reaction products and reducing the high cost of precious metals is still challenging. This review describes the recent development of heterogeneous catalysts for alkene, alkyne, and allene hydrosilylations, which can effectively solve problems in homogeneous hydrosilylation.



## 1. Introduction

Organosilicon compounds are an important class of compounds, which are widely used in materials science, medicinal chemistry, and organic synthesis [1–8]. At present, many research methods have been developed for the synthesis of silicon-containing compounds [9]. Among them, hydrosilylation reactions of unsaturated bonds, such as alkene and alkyne, are studied intensively due to the high atomic economy and wide range of starting materials. In 1947, Sommer reported the peroxide catalyzed the addition reaction of trichlorosilane to 1-octene [10]. In the 1950s, Speier's catalyst was developed as a very effective homogeneous catalyst, which was a big breakthrough in hydrosilylation reactions [11]. The Karstedt's catalyst, which showed high activity with wide substrate scope was reported in 1973 and broadly used in silicone industrial production [12]. Later, transition metals based homogeneous catalysts, such as rhodium, platinum, palladium, ruthenium, and even non-noble metal cobalt, nickel and iron [13], have been widely studied to improve the catalytic performance and reduce the cost. Besides, homogeneous rare-earth metals complexes such as samarium, scandium, yttrium and lanthanum are also developed for the unsaturated bonds hydrosilylations [14–22]. Ligand is very important for homogeneous catalysis while it can influence the activity. Most ligands for the hydrosilylations are expensive and sensitive. On the other hand, the catalysts in homogeneous catalysis are difficult to separate from the reaction mixture and reuse. Therefore, it is still a challenge to find a more excellent catalytic system to achieve high-efficiency and low-cost hydrosilylation reactions.

Heterogeneous catalysis is important because it enables large scale in industrial production. Generally, the heterogeneous catalysts can be recovered easily and reused with long lifetimes. This will reduce the cost of catalysts, especially noble metals, and simplify the separation process effectively. The existence of this driving force has led to a great deal of research in the field of exploring heterogeneous hydrosilylations. Supports are crucial for the activity and selectivity of the reactions. The most popular supports for the catalyst preparation are silica, carbon, metal oxide, organic polymer and metal-organic-frameworks (MOFs).

In this review, we summarized the recent development of heterogeneous catalysts for alkene, alkyne, and allene hydrosilylations. We focus on the following support-based catalysts: silicon, molecular sieve, carbon material, metal oxide, organic polymer, and MOFs materials.

## 2. Silica based catalyst

In 2003, Fang *et al.* prepared a silica-supported Karstedt (Pt)-type catalyst with high catalytic activity for hydrosilylation $Me_2PhSiH$ with styrene at room temperature [23]. Vinylsiloxane groups could bond to the surface of fume silica after the treatment vinyltriethoxysilane. Then treatment with an aqueous solution of

* Corresponding authors.
*E-mail addresses:* ctang@hust.edu.cn (C. Tang), feng.chen@yzu.edu.cn (F. Chen).

https://doi.org/10.1016/j.cclet.2023.109257
1001-8417/

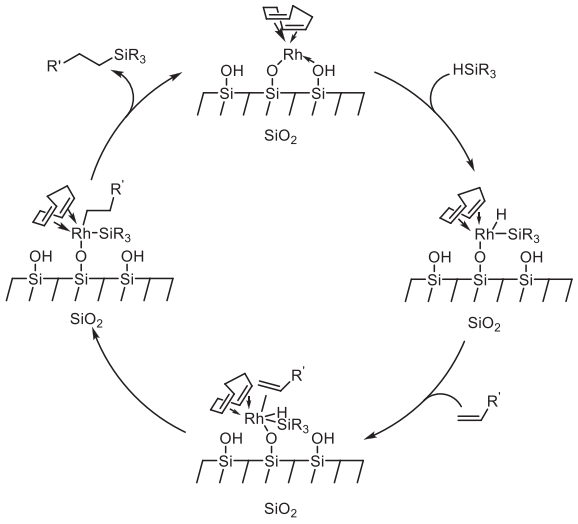

**Fig. 1.** Mechanism of hydrosilylation by surface rhodium(diene)siloxide complex.

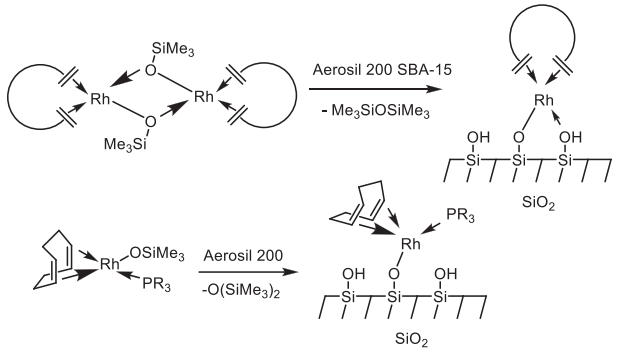

**Fig. 2.** The synthesis of cyclooctadiene rhodium complex loaded on the surface of silicon dioxide.

$H_2PtCl_6$ gives the corresponding heterogeneous Karstedt-like catalyst. The recyclability of this catalyst is also good, and no significant loss of catalytic activity after five runs.

In 2008, Marciniec *et al.* reported cyclooctadiene ligand-containing rhodium siloxide complex immobilized with silanol groups on silica surface Aerosil 200 [24,25]. This single-site complex showed good activity in hydrosilylation of heptamethyltrisiloxane with 1-heptene, vinylheptamethyltrisiloxane and methyleugenol. It offered 20 recycling runs without loss of activity and selectivity in hydrosilylation of vinylheptamethyltrisiloxane with heptamethyltrisiloxane. The detailed mechanism studies disclosed that the pathway of hydrosilylation catalyzed by silica-supported rhodium siloxide complexes is different from homogeneous complexes system (Fig. 1). In 2009, the mononuclear rhodium-silica-phosphine precursor was also used to fix on the surface of silica Aerosil 200 [26]. The catalytic activity in the hydrosilylation of 1-hexadecene with heptamethyltrisiloxane was higher than that of the catalyst without phosphorus ligand, and the catalytic activity did not decrease after 10 cycles (Fig. 2).

In 2017, Motokura *et al.* modified the catalyst of cyclooctadiene rhodium complex loaded on the surface of silicon dioxide, introducing tertiary amine ligand on its surface, which can provide electrons to rhodium complex and promote oxidation addition and insertion steps [27]. The catalyst can catalyze the hydrosilylation reaction of long-chain alkenes with various silanes. Within 24 h, the TON is close to 1900000, showing higher activity than the cat-

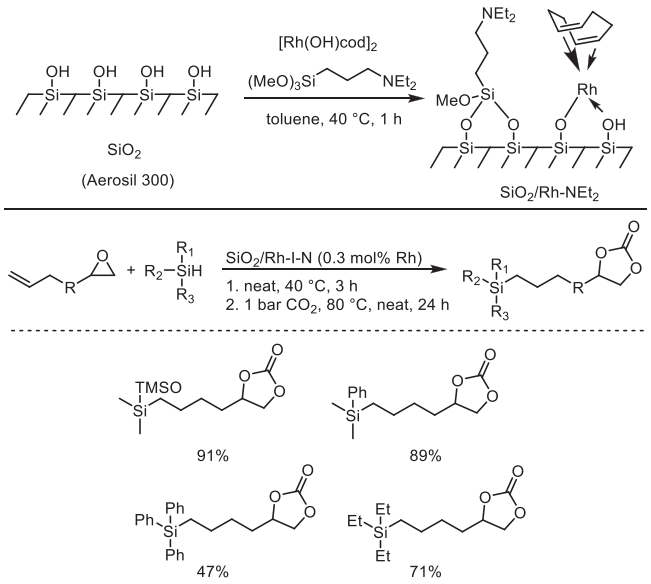

**Fig. 3.** The synthesis of dual-functional catalyst by loading rhodium complex and iodized quaternary ammonium salt on silicon dioxide.

alyst without tertiary amine ligand. And it can still maintain high activity after five cycles. In order to explain the effect of the introduction of tertiary amine on the structure and reactivity of the rhodium complex on the surface, several spectroscopic techniques, such as Rh K-edge XAFS measurements, dynamic nuclear polarization enhanced solid-state $^{15}N$ NMR spectroscopy, and *in situ* FTIR analyses were performed [28]. It is found that the immobilization of amine can significantly improve the dissociation of ligand COD, and the change of COD microstructure can greatly affect the dissociation of rhodium, which can promote the process of ligand exchange, including the insertion of hydrogen-silicon bond, so as to improve the activity of catalyst. In 2019, they synthesized a dual-functional catalyst by loading rhodium complex and iodized quaternary ammonium salt on silicon dioxide [29]. The catalyst can realize one-pot hydrosilylation and cycloaddition reaction of carbon dioxide. Mechanism studies indicate that the increase in the rate of hydrosilylation reaction may be due to the dissociation of COD ligand and rhodium precursor and the provision of electrons by iodide to rhodium center (Fig. 3) [30].

A fumed silica-supported nitrogenous platinum complex was prepared from cheap $\gamma$-aminopropyltriethoxysilane immobilization, followed by treatment with hexachloroplatinic acid (Fig. 4) [31]. The characterization disclosed an interaction of $NH_2$ groups combining with Pt metal in '$SiO_2$'-$NH_2$-Pt, indicating a coordination bond between N and Pt. It is an efficient catalyst for the hydrosilylation of olefins with triethoxysilane, and it can be reused several times *via* simple filtration without any noticeable activity loss.

Li *et al.* also developed a silica supported ethylenediaminetetraacetic acid (EDTA) platinum complex catalyst $SiO_2$-EDTA-Pt to realize solvent-free hydrosilylation of 1-hexene and methyldichlorosilane with high catalytic activity (Fig. 5a) [32]. This catalyst could be recycled 12 times without noticeable loss of catalytic activity. They reported other similar catalysts by loading Pt onto silica particles modified with polycarboxylic acid groups such as diethylenetriaminepentaacetic acid (DTPA) and nitrolotriacetic acid (NTA) (Figs. 5b and c) [33]. The hydrosilylation activity of linear olefins (1-heptene, 1-octene, 1-decene) or cyclic olefins (cyclohexene, norbornene) with methyldichlorosilane is better than homogeneous platinum catalyst. The Pt catalyst can activate the double bond of olefin to generate the alkene-Pt complex. Then

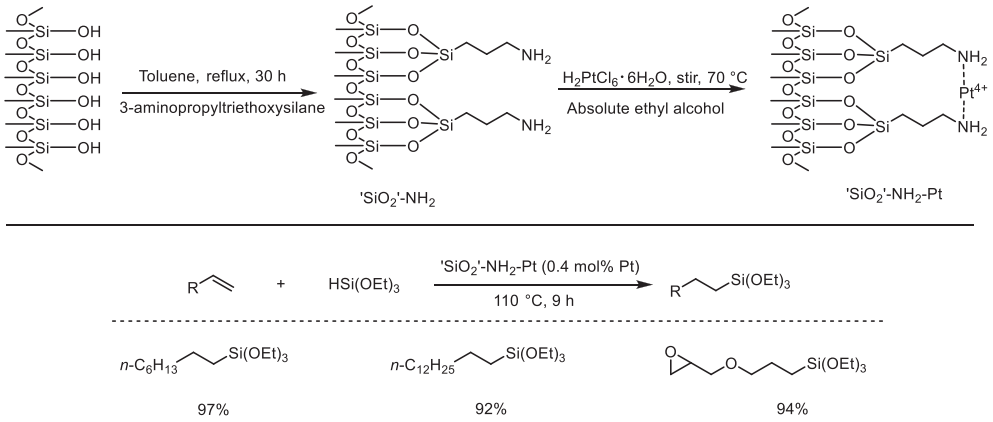


**Fig. 4.** The synthesis of fumed silica-supported nitrogenous platinum complex.

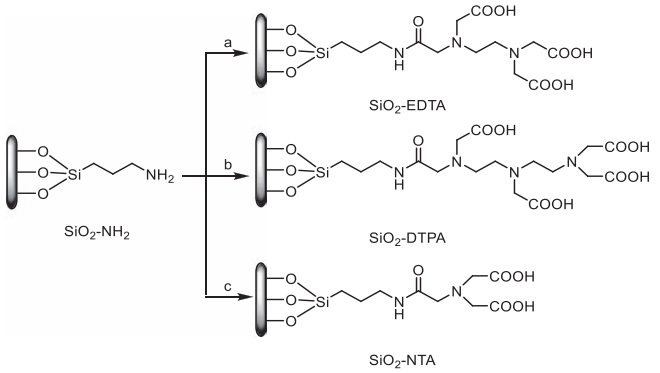


**Fig. 5.** Different ligand modified silica supports.

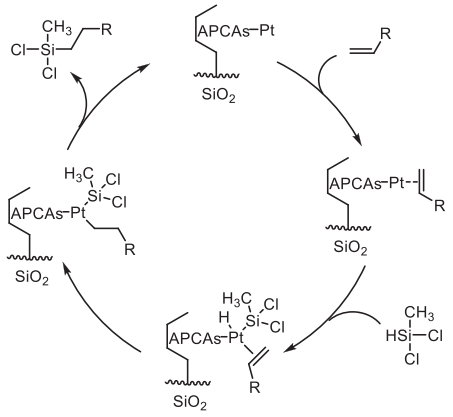


**Fig. 6.** A plausible mechanism for the polycarboxylic acid functionalized Pt catalysts.

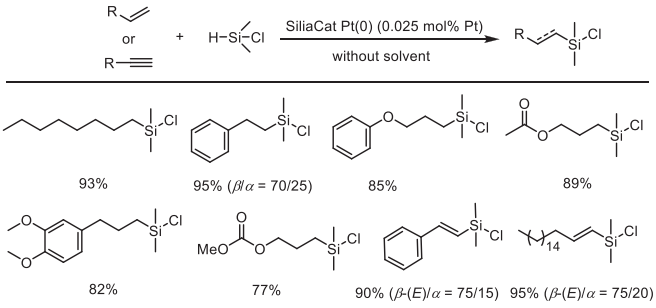


**Scheme 1.** Hydrosilylation of olefins with chlorodimethylsilane over SiliaCat Pt(0).

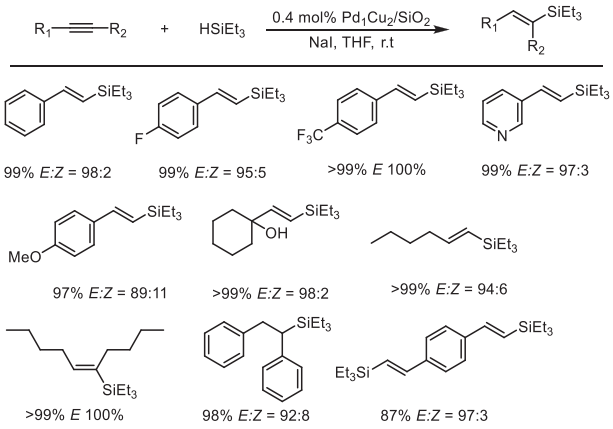


**Scheme 2.** $Pd_1Cu_2/SiO_2$ catalyzed hydrosilylation of alkynes with $Et_3SiH$.

olefin is inserted into the Pt–H bond easily in the presence of methyldichlorosilane (Fig. 6) [34].

Pagliaro *et al.* reported the preparation of 0.5–1.0 mol% Pt(0) nanoparticles (4–6 nm) encapsulated within a sol–gel porous methyl-modified ORMOSIL [35]. This solid catalyst can selectively mediate the hydrosilylation of olefins with triethoxysilane at room temperature or 65 °C. However, the catalyst failed in solvent-free alkene hydrosilylation. In 2019, they reported a silica catalyst with platinum nanoparticles to realize solvent-free alkene hydrosilylation. The substrate scope under this catalytic system is broad (Scheme 1). This catalyst can be recycled several times. By comparing the prepared Pt catalyst with several commercially supported platinum catalysts, it is found that the performance of the catalyst prepared by this method is higher than that of commercial catalysts [36].

A Pd-Cu bimetallic catalyst in an alloy form was synthesized and applied for alkynes hydrosilylation with $Et_3SiH$ without additional ligand [37]. Various vinylsilanes were obtained with excellent yield and selectivity under mild conditions. The arylacetylenes with electron-withdrawing groups show better selectivity than substrates with electron-donating groups (Scheme 2). The extraordinary catalytic performance is attributed to the ultra-small size and homogeneous distribution of the bimetallic nanoparticles. More Pd centers were exposed at the catalyst surface, leading to a low catalyst loading for the hydrosilylation reaction. Furthermore, alloying palladium with cheap copper also can reduce the cost of catalysts, providing better access to green and sustainable chemistry.

## 3. Porous silica based catalyst

In 2010, Cai *et al.* reported a new type of catalyst that immobilized $\gamma$-mercaptopropyltriethoxysilane on mesoporous material MCM-41 followed by treatment with potassium chloroplatinate (MCM-41-SH-Pt) (Fig. 7a). The catalyst is effective for the hydrosilylation reaction between olefin and triethoxysilane [38]. Later, they reported another heterogeneous catalyst with bidentate phosphine rhodium complexes immobilized on $\gamma$-aminopropyltriethoxysilane modified MCM-41 (MCM-41-2P-$RhCl_3$) (Fig. 7b) [39]. The catalyst effectively catalyzes the hydrosilylation reaction of olefin and triethoxysilane. The catalyst can be recovered by simple filtration. Compared with MCM-41-supported mercapto or thioether rhodium complexes, MCM-41-2P-$RhCl_3$ catalyst showed higher activity and better reusability.

Matsuoka *et al.* immobilized cyclopentadienyl ruthenium(II) complex on the surface of aminopropyl-modified MCM-41 (MCM-41-NHCOCpRu$^+$Bz) (Fig. 8) [40]. The catalyst catalyzed the hydrosilylation of 1-hexyne with triethylsilane to vinylsilanes in acetonitrile under UV-light irradiation with high $\alpha$-selectivity. After recycling, the catalytic activity of the catalyst did not lose significantly. The reaction proceeds through *in situ* generations of the corresponding acetonitrile complex as catalytically active species *via* ligand exchange reaction. Recently, they reported another catalyst with organoruthenium complex supported on MCM-41. Compared with the same kind of catalyst without carbonization treatment on the surface for hydrosilylation reaction of 1-hexyne and triethylsilane, the catalyst can improve the ratio of $\alpha$-vinylsilane produced [41].

SBA-15 is another common and highly stable mesoporous silica sieve. Tu *et al.* reported a new type of heterogeneous catalyst by immobilization of platinum-bearing naphthalenolimine and 1,5-cyclooctadiene on the surface of SBA-15 (SBA-15-Naphth-Pt(COD)) (Fig. 9) [42]. The binary ligands also enabled the platinum atoms

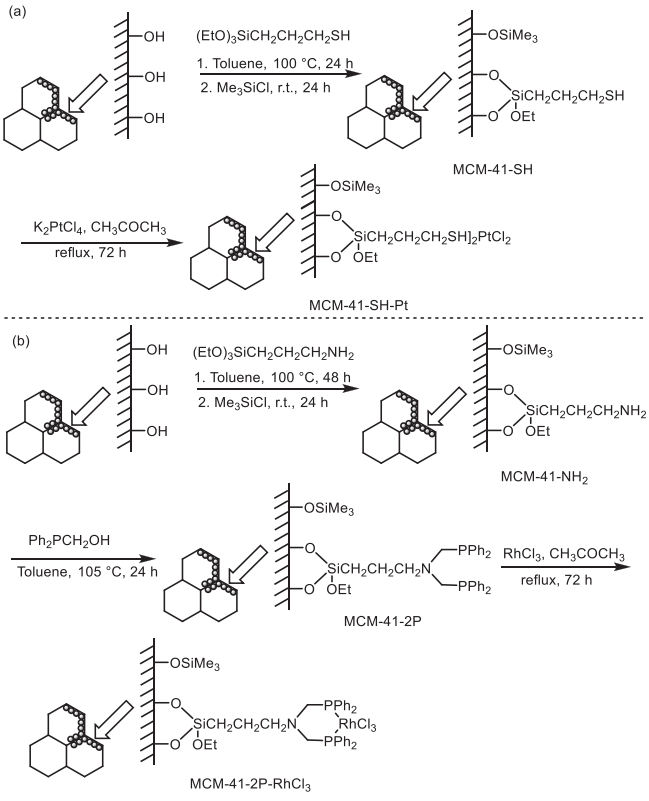


**Fig. 7.** Preparation of the MCM-41-SH-Pt and MCM-41-2P-$RhCl_3$ complexs.

to form nanoclusters (*ca.* 1 nm), leading to high platinum loading of 8.69 wt%, which is higher than most immobilization platinum catalysts. The catalyst showed excellent catalytic activity and regioselectivity for the hydrosilylation of terminal olefins with trimethoxysilane. However, the recyclability of this catalyst is poor.

In 2017, Meille *et al.* reported a catalyst Pt@{walls}SBA-15 with Pt nanoparticles in the walls of mesostructured silica (Fig. 10) [43]. This catalyst showed high activity for the hydrosilylation of polymethylhydrosiloxane with 1-octene reaching TONs of *ca.* $10^5$ without Pt leaching in the reaction. The absence of leaching was attributed to the physical trapping of the Pt NPs in the silica matrix. At the same time, the reactants are close to the active center *via* the microporosity of the support. The good performance indicates that this catalyst could be used in the pharmaceutical industry.

Kónya *et al.* reported platinum catalysts supported by SBA-15 with a size between 1.6 mm and 7.0 nm. The catalyst with 7.0 nm platinum nanoparticles was about 10 times higher than that with 1.6 nm for hydrosilylation reaction of phenylacetylene and triethylsilane. The increase in the size of the nanoparticles increases the yield of vinyl silane products and reduces the by-products [44].

Recently, Shu *et al.* reported a bifunctional heterogeneous catalyst $Pt^{\delta+}$/SBA-APTE-SA *via* post-synthesis modification of (3-aminopropyl)triethoxysilane (APTE), succinic anhydride (SA) and platinum precursors (Fig. 11) [45]. This $Pt^{\delta+}$/SBA-APTE-SA catalyst has a partial valence electron structure and a high degree of dispersion of the Pt species as a catalytic active site for alkenes hydrosilylation. This catalyst is highly stable and shows excellent reusability, maintaining 82% activity after five cycles.

The immobilization of homogeneous catalysts on magnetically recoverable solid supports is a powerful tool for collecting catalyst from the reaction mixture. This process will eliminate conventional separation techniques for catalyst recoveries, such as filtration or centrifugation.

Li *et al.* took $Fe_3O_4$ nanoparticles as the core and coated the silica shell by the inverse microemulsion method to form superparamagnetic $SiO_2/Fe_3O_4$ nanoparticles (Fig. 12). Ultrasmall Pt NPs were prepared through the induced nucleation, possibly by hydrophilic hydroxyl groups on the surface of the silica shell, to form $Pt/SiO_2/Fe_3O_4$ NPs [46]. The synthesized catalyst has high catalytic activity for the hydrosilylation reaction of allyl polyether with low-hydrogen silicone oil. The catalyst dispersed in the reaction solution exhibits a superparamagnetic response under the action of a magnetic field and can be recycled seven times without significant loss of catalytic activity.

Fang *et al.* immobilized 3-aminopropyltriethoxysilane on the surface of $Fe_3O_4$@$SiO_2$ followed by a reaction with chloroplatinic acid, giving a solid-supported Pt catalyst [47]. This catalyst exhibits excellent catalytic performance in the hydrosilylation of olefins with triethoxysilane. The magnet could recover the catalyst quickly and reuse it for several runs without significant catalytic activity and selectivity loss.

Li *et al.* synthesized another superparamagnetic $Fe_3O_4$-$SiO_2$ core-shell nanoparticles supported heterogeneous platinum catalyst [48]. The $SiO_2$ shell layer is modified by a vinyl-containing silane to fix platinum on the surface. This catalyst exhibited high activity in the hydrosilylation reaction of allyl-terminated polyether with polymethylhydrogensiloxane.

In 2019, heterogeneous platinum nanocatalysts through platinum immobilized on magnetic silica gel through boric acid, nitric acid, carboxylic acid, or sulfuric acid ligands were reported by Bao and co-workers [49]. $Fe_3O_4$@$SiO_2$-BA@Pt shows the best catalytic activity and selectivity for hydrosilylation of various alkenes and alkynes with methyldichlorosilane or triethoxysilane. The activity is even better than Speier's catalyst. $Fe_3O_4$@$SiO_2$-BA@Pt showed outstanding stability under reaction conditions. They also prepared platinum catalysts immobilized on superparamagnetic sil-

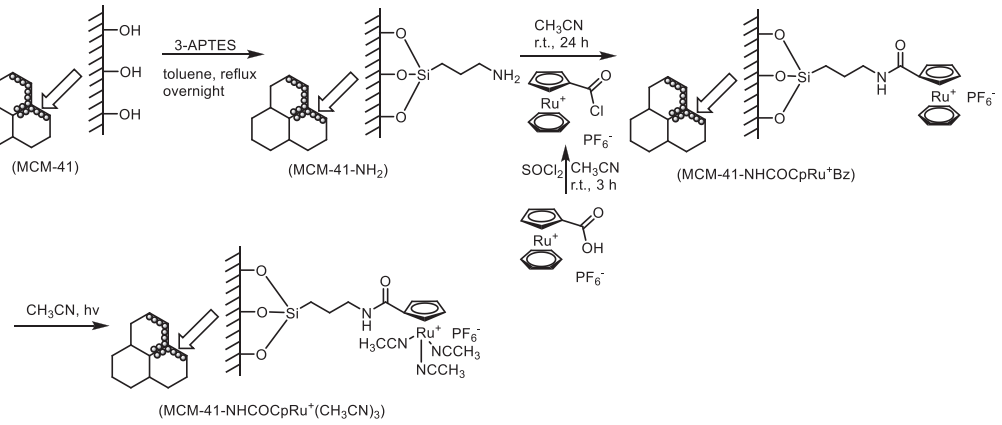


**Fig. 8.** Immobilisation of the cyclopentadienyl ruthenium complex onto MCM-41.

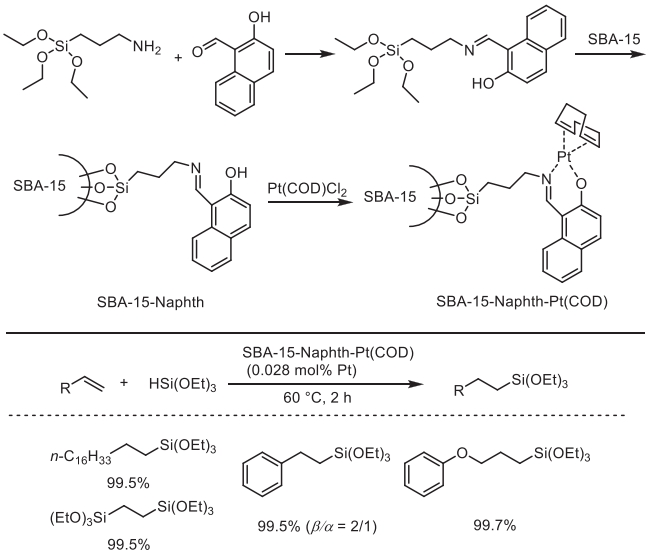


**Fig. 9.** Synthetic pathway to SBA-15-Naphth-Pt(COD).

ica through a multi-carboxyl linker for hydrosilylation of alkenes with methyldichlorosilane [50]. These platinum nanoparticle catalysts exhibit unusual activity and selectivity.

Recently, Feng *et al.* used $Fe_3O_4/SiO_2$ solid support which was modified with aminopropyltriethoxysilane and bis(imidazole)aldehyde to react with $PtCl_2$ through coordination reaction, leading a magnetically separable heterogeneous catalyst $Fe_3O_4$@$SiO_2$-biIMI-$PtCl_2$ [51]. This catalyst can catalyze the hydrosilylation reaction between alkenes and silanes with mainly $\beta$-addition products.

Maciejewski *et al.* prepared a new type of ion-loaded liquid phase material using magnesium oxide-silica and magnesium oxide-silica/lignin as carriers. The homogeneous rhodium and platinum complexes were immobilized in these new supports to generate active hydrosilylation catalysts [52]. These catalysts showed good activity for 1-octene hydrosilylation with 1,1,1,3,5,5,5-heptamethyltrisiloxane, and it can be reused for several runs.

In 2019, Nakajima *et al.* used $[PtMe_2(\mu\text{-}SMe_2)]_2$ as Pt precursor and loaded on BPy PMO carrier to synthesize [$PtMe_2$ (bpy PMO)] (Fig. 13) [53]. This catalyst is used for the hydrosilylation of phenylacetylene and trimethoxysilane. The reaction has the same catalytic activity as the homogeneous catalyst. The main products are $\beta$-vinyl silane in *trans* configuration. After 5 cycles of catalyst, the yield slightly decreased, but the selectivity remained unchanged. The catalyst after 5 cycles was characterized, and the mesoporous structure of the catalyst remained and no aggregation of Pt complex was found.

## 4. Carbon material based catalyst

Graphite oxide (GO) is an inexpensive and stable material [54]. The carbons or at the edges of the layer always have various oxygen-containing functional groups, indicating that they can be modified with compounds containing active groups. Therefore, graphite oxide is an ideal supporting material for homogenous catalyst immobilization.

In 2013, Zhang *et al.* immobilized vinyltriethoxysilane on graphite oxide and reacted with chloroplatinic acid to synthesize a graphite oxide-supported heterogeneous Karstedt catalyst (Fig. 14). The catalyst has a good activity for the hydrosilylation of olefins and triethoxysilane with good recyclability. No noticeable loss of activity and selectivity was found after being reused seven times [55].

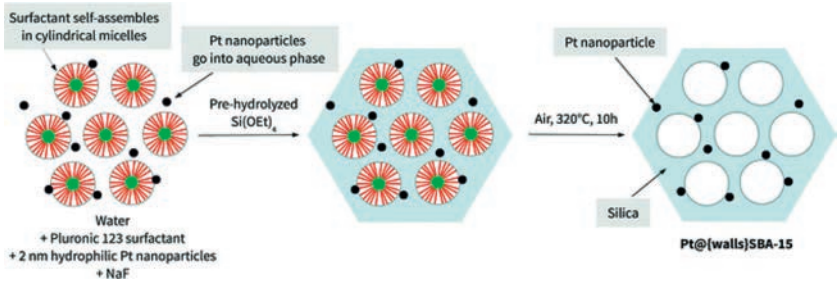


**Fig. 10.** Synthesis of Pt@{walls}SBA-15. Copied with permission [43]. Copyright 2017, Royal Society of Chemistry.

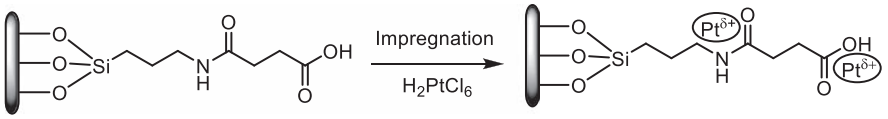


**Fig. 11.** The synthesis of $Pt^{\delta+}$/SBA-APTE-SA catalysts.

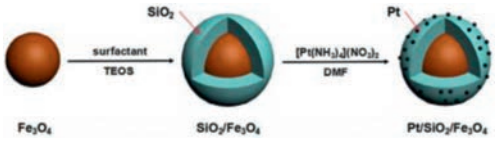


**Fig. 12.** Schematic showing the synthetic protocol of the $Pt/SiO_2/Fe_3O_4$ catalyst. Copied with permission [46]. Copyright 2016, Royal Society of Chemistry.

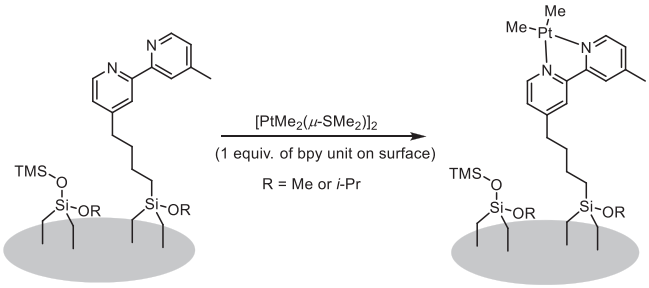


**Fig. 13.** The synthesis of $[PtMe_2(bpy\ PMO)]$ catalyst.

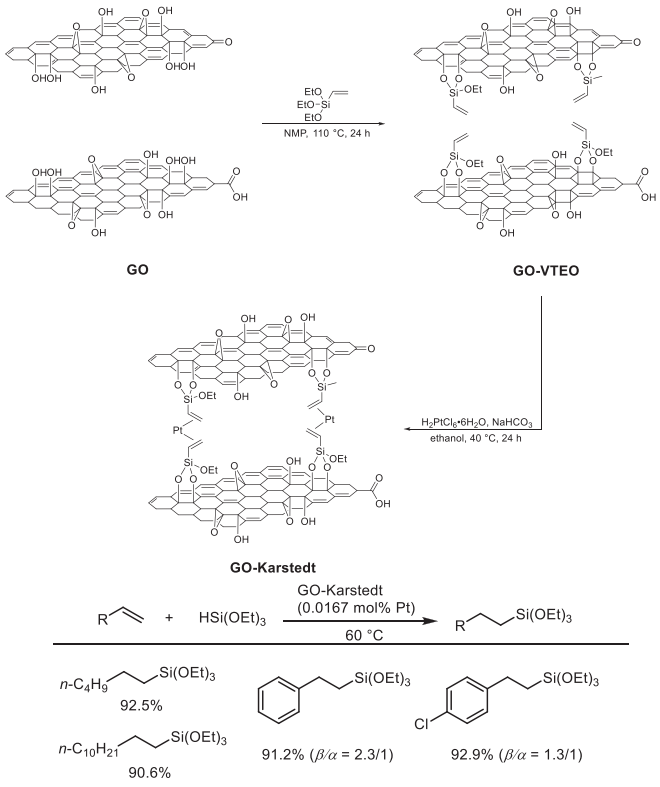


**Fig. 14.** The construction of GO-Karstedt catalyst and application for the hydrosilylation of olefins and triethoxysilane.

Gupton *et al*. combined the strong electrostatic adsorption technology and microwave radiography to prepare graphene-supported platinum catalyst, which shows excellent catalytic activity and stability for hydrosilylation reactions of olefins (TOF $4.8 \times 10^6$ $h^{-1}$, TON $= 9.4 \times 10^6$) [56]. The catalyst also exhibited good functional group tolerance with a broad range of substrate scope with minimal metal leaching (Scheme 3). Moreover, The packed bed platform for continuous hydrosilylation reactions is also successfully performed.

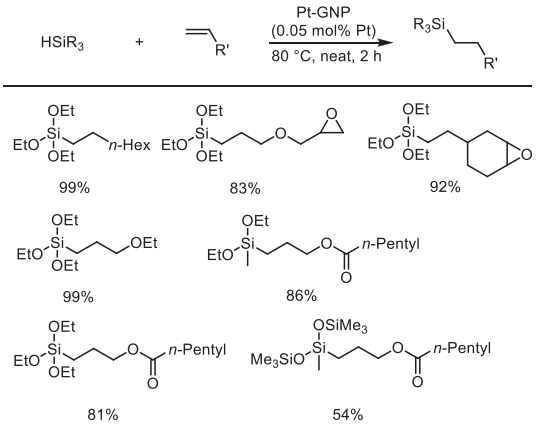


**Scheme 3.** Graphene-supported platinum catalyst for alkene hydrosilylation.

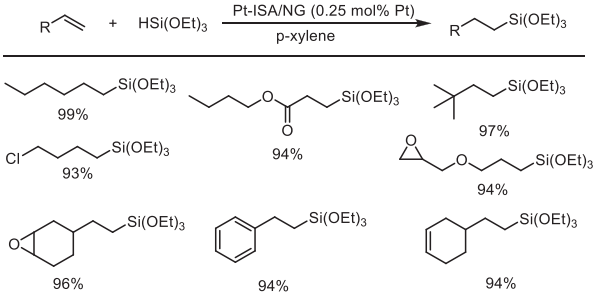


**Scheme 4.** Hydrosilylation of alkenes with triethoxysilane by Pt-ISA/NG catalyst.

Li *et al.* developed an ammonium carbonate-assisted one-pot pyrolysis of EDTA-Pt complex to afford high-density isolated platinum single-atom sites, which are restricted to nitrogen-doped graphene with a platinum content of 5.3% by weight (Pt-ISA/NG) [57]. Characterization shows that Pt species are atomically dispersed on graphene support and stabilized by nitrogen in $Pt–N_4$ structure. The catalyst shows high selectivity, reactivity, and recyclability for the anti-Markovnikov hydrosilylation of various terminal olefins with industrially relevant tertiary silanes under mild conditions (Scheme 4). The catalytic efficiency of the catalyst is four times higher than that of a 5 wt% commercial Pt/C catalyst. Pt-ISA/NG catalyst is stable under air, and the substrate scope is broad. Therefore, this Pt-ISA/NG is a promising catalyst for the synthesis of commercially relevant silicone.

Later, they successfully prepared nano-PtNi particles on nitrogen-doped carbon (NC) through carbonization of ZIF-8 at different temperatures (Fig. 15) [58]. For the hydrosilylation of 1-octene with $(EtO)_3SiH$, the catalyst prepared at 1000 °C (nano-PtNi/NC-1000) exhibited higher anti-Markovnikov selectivity (>99%) than the catalyst obtained with lower temperatures. Notably, this nano-PtNi/NC-1000 catalyst showed good reusability for the hydrosilylation reaction. The morphology and distribution of

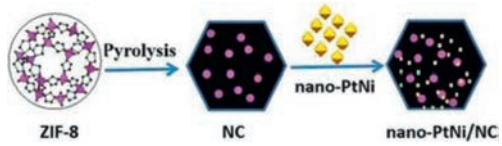


**Fig. 15.** The illustration of the synthesis of nano-PtNi/NC. Copied with permission [58]. Copyright 2019, Springer Nature.

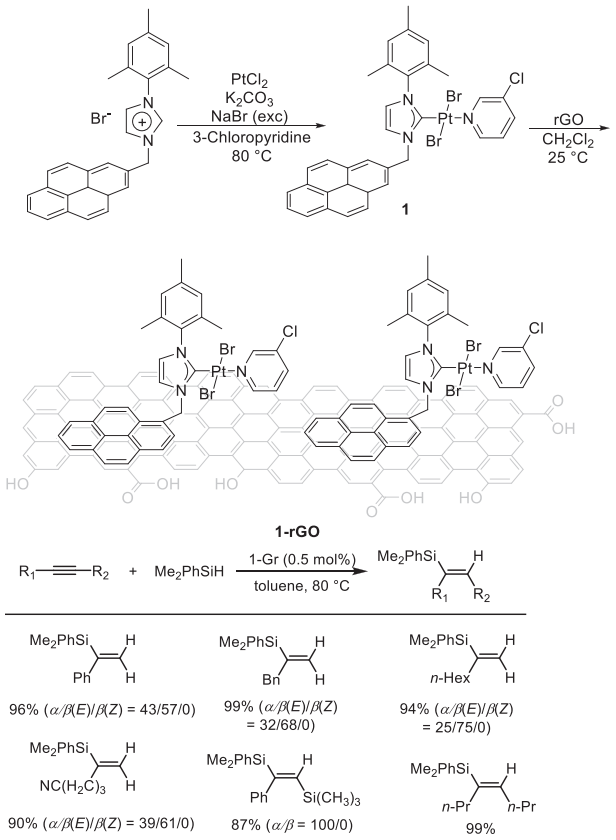


**Fig. 16.** Synthesis of the platinum complex and the hybrid material 1-rGO.

PtNi particles in nano-PtNi/NC-1000 catalyst almost remained after use.

In 2020, Mata *et al.* immobilized platinum complexes with heterocyclic carbene ligands onto the surface of reduced graphene oxide (rGO) (Fig. 16) [59]. This hybrid material composed of a platinum complex and a graphene derivative was prepared in a single-step process under mild reaction conditions. The platinum sites were homogeneously distributed at the edges of defects. The alkyne hydrosilylation activity of the immobilized platinum catalyst is maintained, and the reaction rate is even greater than platinum complexes. The support plays an important role and may bring the close of substrates with the platinum sites at the graphene surface.

A $PtFe_3$ intermetallic catalyst anchored on N-doped carbon spheres ($PtFe_3$/CN) *via* an *in-situ* location-restricted migration (LRM) strategy was developed by Huang and co-workers recently [60]. The electron-rich nature of Pt sites could be attributed to the low electronegativity of iron atoms' coordination. This $PtFe_3$/CN catalyst gave better activity for the alkene hydrosilylation with high selectivity for anti-Markovnikov addition than traditional single-atom Pt catalyst loading on N-doped graphene carbon and Pt nanoparticles supported on N-doped carbon spheres (Scheme 5). The turnover number (TON) of alkene hydrosilylation can reach 740,000, and no platinum leaching occurs. Lvarez *et al.* synthe-

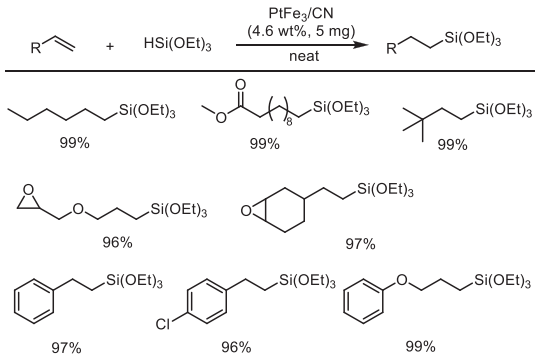


**Scheme 5.** Hydrosilylation of alkenes with $(EtO)_3SiH$ catalyzed by $PtFe_3$/CN catalyst.

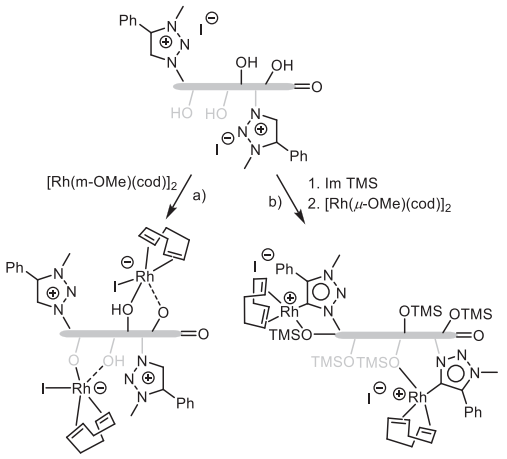


**Fig. 17.** Synthesis of graphene−NHC−rhodium hybrid catalysts.

sized graphene−NHC−rhodium hybrid catalysts from thermally reduced graphene oxides [61]. The 3-methyl-4-phenyl-1,2,3-triazole salt was used to modify the reduced graphene oxides leading to hydroxyl-triazolium-functionalized materials. The final obtained rhodium hybrid materials contain either alkoxo or triazolylidene molecular rhodium(I) complexes depending on the protection of the hydroxyl groups. Catalyst characterization disclosed the coordination sphere of the supported rhodium(I) complexes in rhodium hybrid materials (Fig. 17). This graphene oxide-supported rhodium catalyst exhibits excellent activity for the hydrosilylation of terminal and internal alkynes. Moreover, these supported rhodium catalysts showed good selectivity to $\beta$-($Z$) vinylsilane isomers (terminal substrates) or *syn*-additions (internal substrates).

Carbon nanotubes (CNTs) are carbon materials that could be used as support for heterogeneous catalysis preparation. Doris and co-workers reported a heterogeneous platinum-based catalyst based on a carbon nanotube platform [62]. The obtained catalyst (0.04 mol% catalyst loading) showed excellent activity for the solvent-free hydrosilylation of alkenes and alkynes at room temperature. The substrate scope is broad, including complex molecules bearing sensitive groups, and its recycling ability is good (Fig. 18).

Atomically dispersed Au anchored on g-$C_3N_4$ nanosheets is developed by Chen *et al.* [63]. The atomic Au species are in the +1 oxidative state, coordinating with three nitrogen atoms *via* X-ray absorption fine structure (XAFS) characterization. Gold sites' unique structural and electronic characteristics are crucial for the activation of Si–H bonds. Aromatic alkynes and aliphatic alkynes can effectively produce corresponding $\beta$-($E$)-vinylsilane products with high yields and functional group tolerance (Scheme 6). This

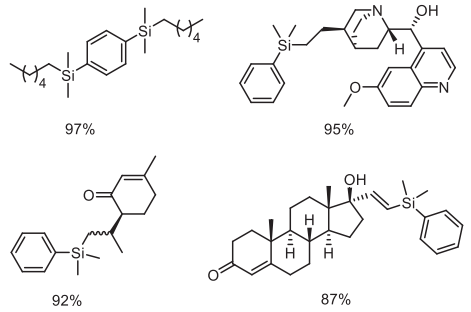


**Fig. 18.** Examples of PtCNT-based hydrosilylation on structurally challenging substrates

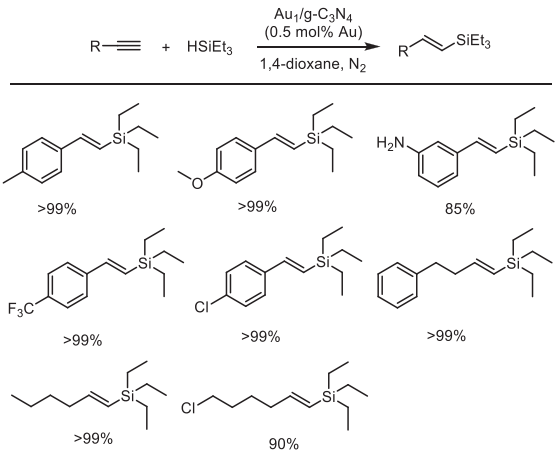


**Scheme 6.** Scope of hydrosilylation reaction with $Au_1/g\text{-}C_3N_4$ nanosheets.

Au catalyst could be reused at least five times without obvious loss in activity and selectivity.

## 5. Metal oxide based catalyst

Metal oxides are ideal supports for the preparation of the catalyst and have been widely applied in industrial production. The commonly used metal oxide carriers mainly include alumina oxide, magnesium oxide, cerium oxide, titanium oxide, *etc.* Most of the metal oxide supported catalysts for alkene and alkyne hydrosilylation are based on palladium, rhodium, and platinum.

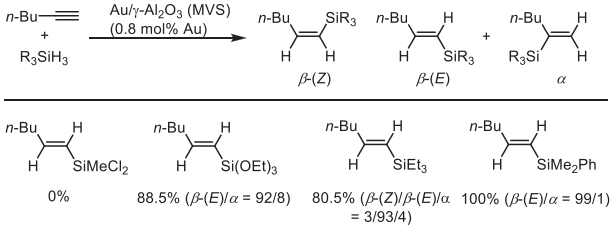


**Scheme 7.** $Au/\gamma\text{-}Al_2O_3$ catalyst for hydrosilylation of 1-hexyne with different silanes.

Catalysts prepared through the sol-gel method have been well developed, and these catalysts generally show good catalytic activity for various organic reactions. In 2000, Cervantes and coworkers reported catalysts based on Pt and Ru supported on inorganic matrices MgO through the sol-gel process. These Ru–MgO and Pt–MgO catalysts are able to catalyze hydrosilylation of phenylacetylene with $Ph_3SiH$, $Ph_2MeSiH$, and $PhMe_2SiH$, leading to a specific activity and good selectivity (Fig. 19) [64].

In 2005, Caporusso *et al.* developed supported gold nanoparticles using the metal vapour synthesis (MVS) technique [65]. The catalysts were prepared by depositing acetone solvated Au atoms on different supports, such as $\gamma\text{-}Al_2O_3$ and carbon. These catalysts are very efficient for the hydrosilylation of 1-hexyne with different silanes. Almost 100% selectivity towards the $\beta$-(*E*) isomer was obtained (Scheme 7). These merits make these gold-based catalysts a good alternative to more expensive Pt-based catalysts for the alkyne hydrosilylations through this heterogeneous synthetic process.

Corma *et al.* reported that $CeO_2$ nanoparticles could stabilize cationic forms of gold ($Au^I$ and $Au^{III}$) [66] in 2002. Later, they found that this gold supported on $CeO_2$ catalyst can catalyze the hydrosilylation of aldehydes, ketones, olefins, imines, and alkynes with excellent selectivity [67]. This catalyst can be recycled successfully without any loss of activity. Mechanism studies disclosed that the presence of stabilized $Au^{III}$ on the surface $Au/CeO_2$ is crucial for these hydrosilylation reactions.

In 2012, a catalyst of gold nanoparticles supported on titanium oxide (0.8-1.4 mol%) catalyst was reported by Stratakis *et al.* This catalyst can catalyze the $\beta$-(*E*) regioselective hydrosilylation of various functionalized terminal alkynes with alkylhydrosilanes with excellent yields (Scheme 8) [68]. The less hindered triethylsilane and dimethylphenylsilane react faster (2-4 h) than the bulky triphenylsilane. Internal alkynes are less reactive or even unreactive un-

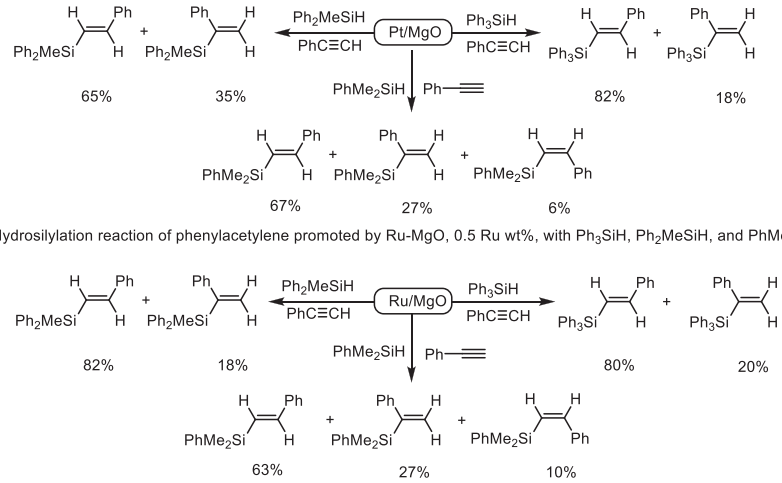


**Fig. 19.** The Ru–MgO and Pt–MgO catalysts for hydrosilylation of phenylacetylene with $Ph_3SiH$, $Ph_2MeSiH$, and $PhMe_2SiH$.

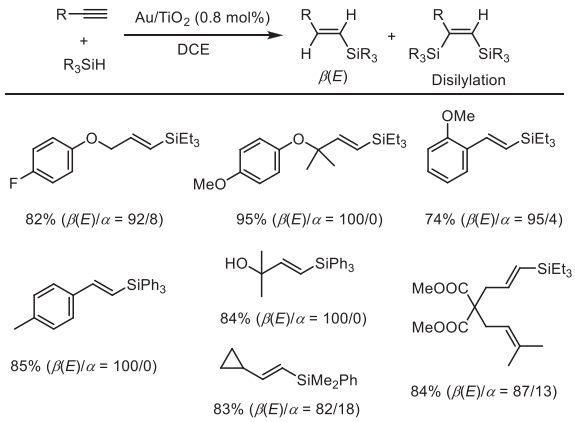


**Scheme 8.** Hydrosilylation of terminal alkynes catalyzed by $Au/TiO_2$.

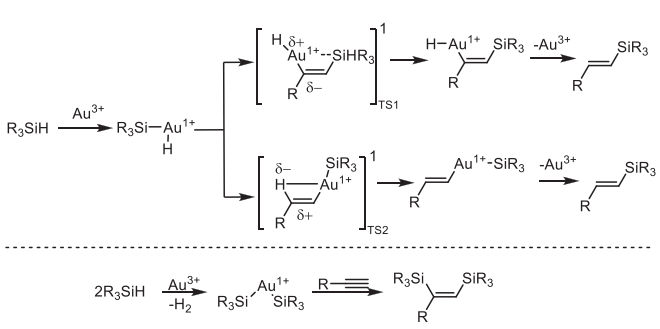


**Fig. 20.** Proposed mechanism for $Au/TiO_2$ catalyzed terminal alkyne hydrosilylation.

der this catalytic system. Mechanism studies disclosed that the $TiO_2$ stabilized cationic $Au^I$ species are the reactive sites, including a $Au^I$-$Au^{III}$ redox catalytic cycle (Fig. 20).

$PtO_2$ is a highly active and regioselective hydrosilylation catalyst for hydrosilylation [69]. Initially, Pt(IV) is reduced to Pt(II) or Pt(0) to generate the active sites, which are soluble in the reaction mixture and could be removed from the product after the reaction. However, only a small amount of Pt sites (<<10 ppm) are needed [70].

The development of low Pt loading and stable catalyst is desired considering the price of the Pt. In 2010, Yus *et al.* demonstrated a $Pt/TiO_2$ catalyst that can catalyze the hydrosilylation of terminal and internal alkynes, bearing different functional groups with three hydrosilanes to give the corresponding alkenylsilanes in high yields under solventless conditions [71]. This catalytic system proceeded with exclusive *syn* addition of hydrosilanes to the C≡C bond, and the $\beta/\alpha$ regioselectivity can reach up to 94:6. In contrast to known heterogeneous platinum catalysts, the present $Pt/TiO_2$ catalyst could catalyze the reaction under air and mild conditions (Scheme 9). Moreover, this catalyst can be easily recovered from the reaction mixture and reused in several cycles without activity loss.

In 2017, Beller and co-workers reported the first heterogeneous single-atom Pt catalyst by decorating alumina nanorods with platinum atoms. This single-atom based heterogeneous platinum catalyst was a selective catalyst for alkene hydrosilylation with high TON ($\sim 10^5$) [72]. Compared to the known heterogenized catalysts, this $Pt/NR\text{-}Al_2O_3\text{-}IP$ catalyst gives high activity and excellent chemoselectivity (Scheme 10). The substrates with sensitive reducible and functional groups are also compatible. Moreover, industrially relevant polysilane PL6020 was tested with 1-octene or vinyl-trimethylsilane (Scheme 11). These reactions proceeded smoothly catalyzed by this single-atom Pt catalyst.

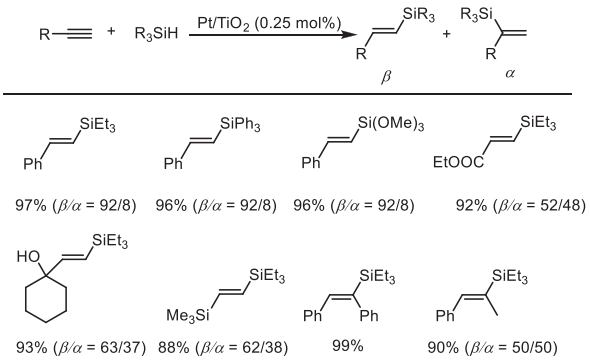


**Scheme 9.** $Pt/TiO_2$ catalyst catalyzed hydrosilylation of alkynes.

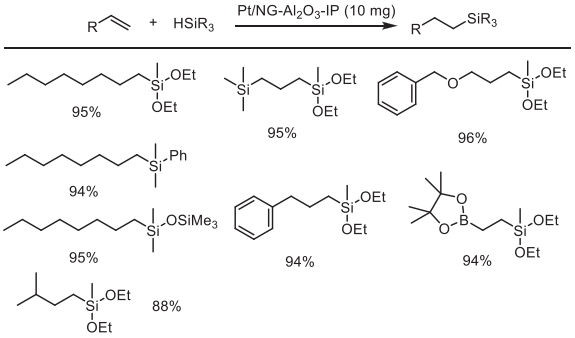


**Scheme 10.** Single atom Pt catalyzed selective hydrosilylation of olefins.

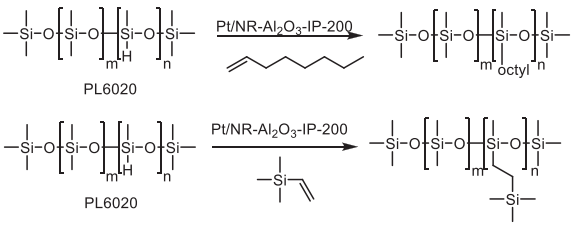


**Scheme 11.** Single atom Pt catalyzed hydrosilylation of industrially relevant polysilane PL6020 with 1-octene or vinyl-trimethylsilane.

In 2018, Miura *et al.* synthesized $1Pd5Au/Al_2O_3$ by doping Pd atoms into Au NP and loading on alumina support [73]. The synthesized catalyst is used for the hydrosilylation of diene with silane, and the main product is internal alkenylsilane with *E* configuration (Scheme 12). The catalyst can still maintain high activity after three cycles. Kinetic experiments showed that the incorporation of Pd atoms into Au NP promoted the coupling of C-H, the rate-limiting step of the reaction, and increased the reaction rate.

Li *et al.* developed a new catalyst with single atomic partially charged Pt sites on anatase $TiO_2$ ($Pt_1^{\delta+}/TiO_2$) *via* electrostatic-induction ion exchange and two-dimensional confinement strategy (Fig. 21) [74]. This catalyst can realize the anti-Markovnikov alkene hydrosilylation with high activity, selectivity, and excellent reusability. The good performance of this catalyst is attributed to the partially positive valence electronic structure and atomic dispersion of Pt sites. The strategy can reduce the consumption of precious platinum in the form of single-atom Pt and has the potential application in the hydrosilylation industry.

In 2019, Tait *et al.* reported a metal-ligand self-assembly process to create Pt single-sites on high surface area supports MgO, $Al_2O_3$, and $CeO_2$ [75]. One-step impregnating Pt and 3,6-di-2-pyridyl-1,2,4,5-tetrazine (DPTZ) simultaneously can generate Pt-DPTZ single-sites on supports. A highly uniform structure, with 90% Pt as single-sites, was obtained on MgO. Pt(II) centers

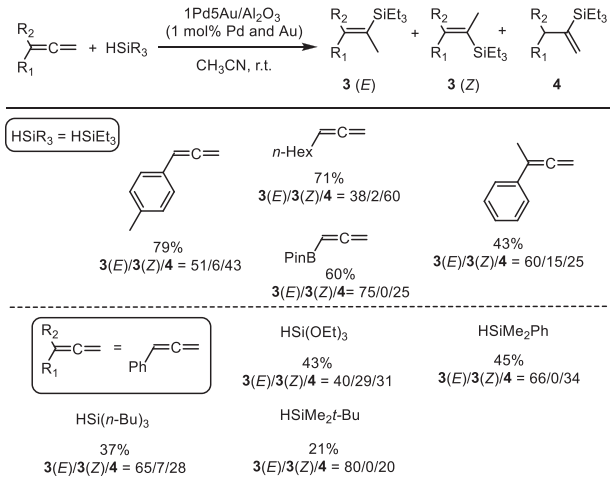


**Scheme 12.** 1Pd5Au/$Al_2O_3$ catalyzed hydrosilylation of diene with silane.

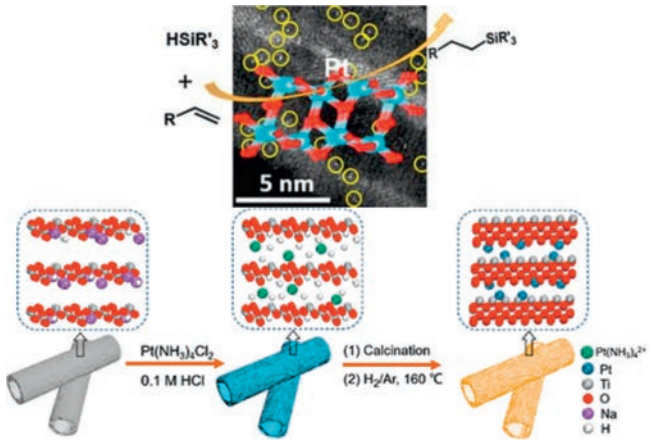


**Fig. 21.** Illustration of Preparation Process of $Pt_1^{\delta+}/TiO_2$. Copied with permission [74]. Copyright 2018, American Chemical Society.

could be stabilized in the DPTZ binding pockets. Strong, non-competitive support-ligand interaction favors the formation of Pt single-sites. However, the catalysts prepared *via* two-step impregnation of Pt and DPTZ are less effective because Pt atoms have low mobility and accessibility on supports. The single-sites Pt-DPTZ/MgO catalyst was effective for 1-octene hydrosilylation with dimethoxymethylsilane in 96% yield (Scheme 13). Compared with commercial homogeneous catalysts, Pt-DPTZ/MgO catalyst has better activity and selectivity without the formation of colloidal platinum.

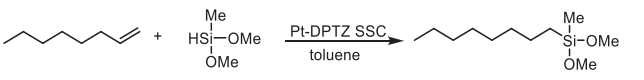


| Catalyst | T (°C) | t (min) | Product yield (%) | 2-Octene yield (%) | Octane yield (%) |
|---|---|---|---|---|---|
| Pt-DPTZ/MgO | 75 | 120 | 96 | 3 | 0 |
| Pt-DPTZ/CeO | 70 | 20 | 91 | 4 | 1 |
| Pt-DPTZ/$Al_2O_3$ | 70 | 20 | 85 | 2 | 0 |
| Speier catalyst | 70 | 20 | 13 | 8 | 13 |
| Karstedt catalyst | 70 | 20 | 86 | 6 | 2 |

**Scheme 13.** Catalytic performances of oxide-supported Pt-DPTZ SSCs and commercial homogeneous catalysts in hydrosilylation reactions between 1-octene and dimethoxymethysilane.

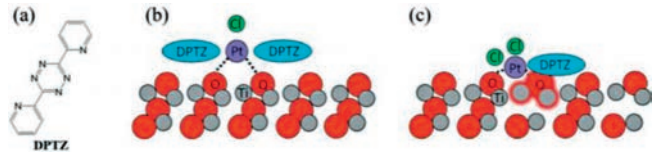


**Fig. 22.** Pt SACs with ligand DPTZ on $TiO_2$. (a) Structure of dipyridyl tetrazine (DPTZ). Schematic illustrations of Pt–DPTZ on (b) pristine $TiO_2$ (101) and on (c) defective $TiO_2$ (with oxygen vacancy). Copied with permission [77]. Copyright 2020, Royal Society of Chemistry.

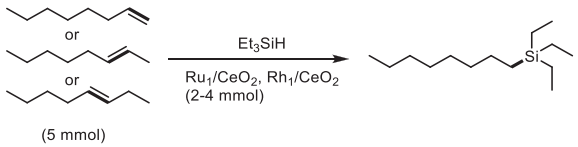


**Fig. 23.** single-atom Rh and Ru on $CeO_2$ for anti-Markovnikov $\alpha$-olefin hydrosilylation.

To improve catalyst's recyclability of previous Pt-DPTZ SACs, they reported a series of bidentate N-based ligand-coordinated supported Pt hydrosilylation catalysts [76]. First, they prepared catalyst Pt-PDO/$CeO_2$ (PDO = 1,10-phenanthroline-5,6-dione) by replacing DPTZ with a ligand PDO containing additional functional groups. This catalyst can proceed for four reaction cycles, and much less Pt leaching occurs. A $Pt^{(2+\delta)+}$ species converted from $Pt^{2+}$ is likely the active site. Second, mixing DPTZ with BPhen leads to a highly reusable catalyst Pt-BPhen+DPTZ/$CeO_2$ which shows only 10% activity decrease after three cycles. The ligand mixing provides additional van der Waals interaction with the support.

They also studied the impact of the defect density of the $TiO_2$ on Pt SACs with ligand DPTZ for hydrosilylation reactions [77]. These Pt species are stabilized by bonding with DPTZ, surface oxygen, and residual chloride from the metal precursor. The activity of catalysts is positively correlated with the defect density of the $TiO_2$ (Fig. 22). The turnover number is 12530 for Pt SACs on a defective surface, which is significantly higher than Pt SACs on a pristine $TiO_2$ surface under the same reaction conditions. The coordination of Pt with more chloride than on pristine titania surfaces will shorten the induction period of the reaction. Besides, the high dispersion of Pt–DPTZ units on defective regions of titania surfaces allows facile contact between Pt sites and reactants. These Pt–DPTZ SACs show high stability through multiple cycles of reactions. Therefore, optimizing the metal–support interaction through the oxide support defect engineering approach can also be applied to other oxide surfaces.

Besides the Pt single-site catalyst, Prieto *et al.* developed a catalyst through a one-pot combination of single-atom Rh and Ru on $CeO_2$ [78]. Individually, Ru/$CeO_2$ and Rh/$CeO_2$ catalysts show specificity for olefin double-bond migration and anti-Markovnikov $\alpha$-olefin hydrosilylation, respectively (Fig. 23). The combination of two single-atom metal catalysts can realize a selective olefin isomerization-hydrosilylation tandem process with high regioselectivity (>95%), including terminal and internal olefins. The catalyst recycling and reuse ability are also good, while no noticeable decrease in either activity or selectivity after five consecutive tandem reaction cycles. DFT calculations ascribe the selectivity to the differences in the binding strength of the olefin substrate to the metal centers. This strategy provides a new method of single-atom metal catalysts in tandem catalysis, which can be a bridge between homogeneous and heterogeneous catalysis.

Very recently, Su and co-workers reported a $0.5Ru^{\delta+}/ZrO_2$ catalyst with partially charged single-atom Ru supported on $ZrO_2$ by the simple impregnation method followed by reduction [79]. This $0.5Ru^{\delta+}/ZrO_2$ catalyst showed excellent catalytic performance for

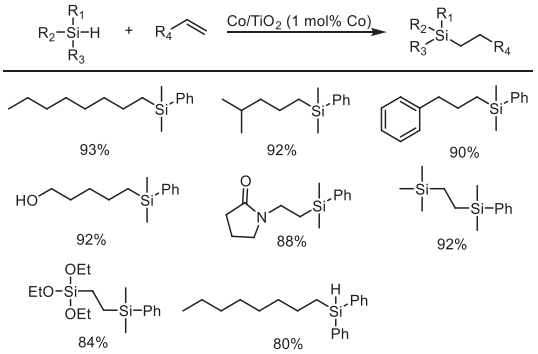


**Scheme 14.** $Co/TiO_2$-catalyzed hydrosilylation of alkenes under solvent-free conditions.

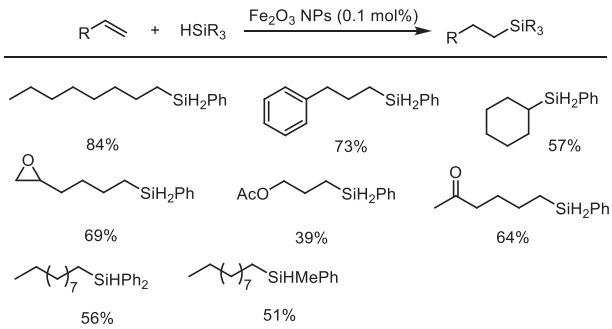


**Scheme 15.** $Fe_2O_3$ NP-catalyzed hydrosilylation of alkenes with hydrosilanes.

ethylene hydrosilylation with triethoxysilane to ethyltriethoxysilane. Notably, poor catalytic performance was obtained using other metal oxides as support, including $0.5Ru/CeO_2$, $0.5Ru/Al_2O_3$, and $0.5Ru/SiO_2$. Structural characterizations and density functional theory calculations reveal that the atomic dispersion of the active Ru species and their unique electronic properties are crucial to realize the high activity for hydrosilylation.

Except for the precious metal, non-noble metal based heterogeneous catalyst was also developed for alkene hydrosilylation. In 2012, Kaneda *et al.* reported an air-stable cobalt ion-doped titanium oxide catalyst by hydrogen treatment method for alkene hydrosilylation under solvent-free conditions [80]. The reported $Co/TiO_2$ catalyst was a highly efficient catalyst for the anti-Markovnikov hydrosilylation of alkenes with broad functional group tolerance (Scheme 14). This catalyst showed high reusability without activity loss after five runs. The detailed investigation of the relationship between the active site and catalytic performance disclosed that the high stability and durability of $Co/TiO_2$ originated from the strong interaction between Co and $TiO_2$ through the formation of $CoTiO_3$ solid solution species.

Obora and co-workers prepared DMF-protected monodisperse $\alpha$-$Fe_2O_3$ NPs (2–5 nm) from Iron(III) acethylacetonate [81]. Characterization disclosed that DMF molecules existed as a tightly protective layer around the $Fe_2O_3$ NPs. The synthesized $Fe_2O_3$ NPs showed good catalytic activity for hydrosilylation of alkenes under additives-free conditions (Scheme 15). No significant deactivation of this DMF-protected $Fe_2O_3$ NPs was observed after the $5^{th}$ run, while the separation and recovery of the $Fe_2O_3$ NPs from the reaction mixture was simple.

## 6. Organic polymer based catalyst

Cross-linked polymers are always used as scaffolds for catalyst preparation. For example, polystyrene is one of the most popular polymers supports because of its facile functionalization and

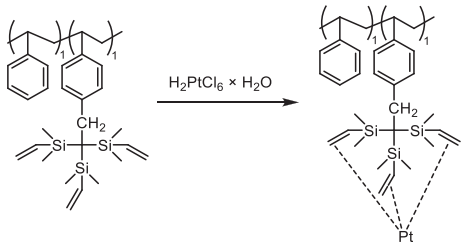


**Fig. 24.** Preparation of platinum catalysts on $V_{Si}$-modified polystyrene supports.

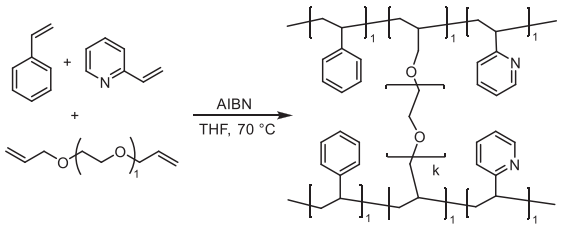


**Fig. 25.** The structural representation of the novel polymer.

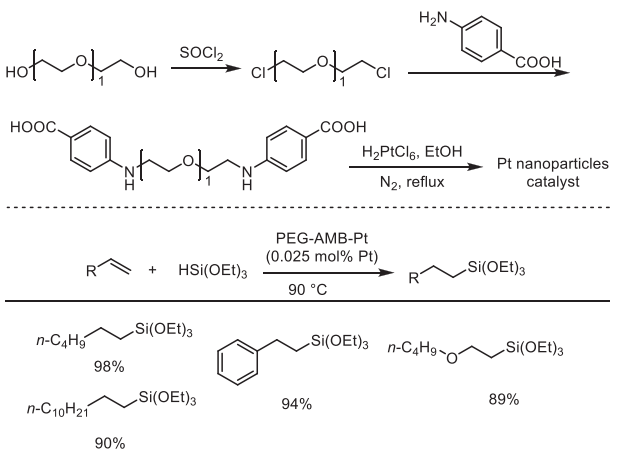


**Scheme 16.** Synthesis of PEG-AMB stabilized Pt nanoparticles catalyst.

chemical inertness. In 2002, Kan *et al.* prepared a cross-linked polystyrene-platinum complex that can catalyze the hydrosilylation of olefins with dichloromethylsilane and diethoxymethylsilane. This catalyst has no catalytic activity for olefins containing two substituents on the double bond [82]. Kowalewska reported a new polymeric support based on tris(dimethylvinyl)methyl substituted polystyrene, which has coordination-active sites ($-CH{=}CH_2$ moieties) (Fig. 24). This polymer-bound platinum complex shows good activity in hydrosilylation of vinylsilanes, which is comparable to the Karstedt's catalyst [83].

Lai *et al.* developed a copolymer of styrene, 2-vinylpyridine, and allyl polyethylene glycol as a cross-linking agent. The copolymer-immobilized platinum showed good activity for hydrosilylation of 3,3,3-trifluoropropene with triethoxysilane [84]. The presence of 2-vinylpyridine and allyl polyethylene glycol in the polymer was crucial to improve the activity (Fig. 25).

They also reported another platinum nanoparticle catalyst stabilized by 4-aminobenzoic acid with functionalized polyethylene glycol (Scheme 16) [85]. These functionalized PEG-stabilized Pt nanoparticles form a very efficient catalyst for alkenes hydrosilylation. The Pt nanoparticles can be fully immobilized in the PEG-AMB and recycled at least nine times without any obvious loss of catalytic activity.

In 2014, a catalyst of palladium nanoparticles stabilized with tris-imidazolium tetrafluoroborates was reported by Pleixats and

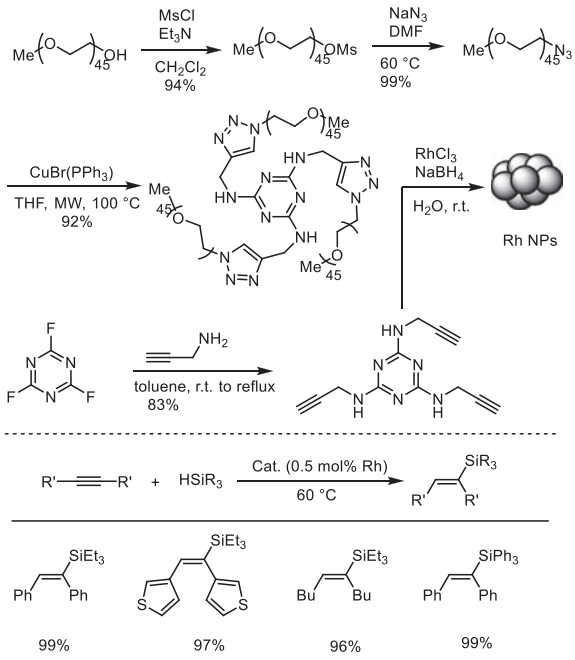


**Fig. 26.** Synthesis of palladium nanoparticles stabilized with tris-imidazolium tetrafluoroborates.

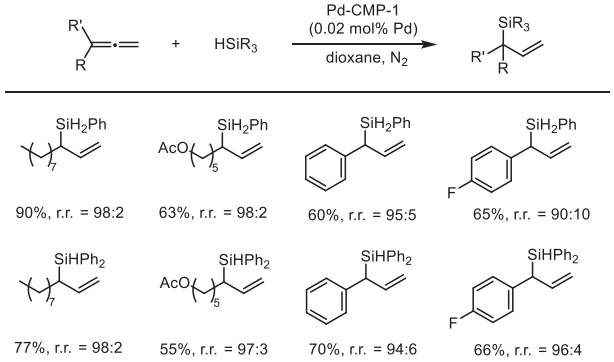


**Scheme 17.** Substrate scope of allene hydrosilylation with Pd–CMP-1.

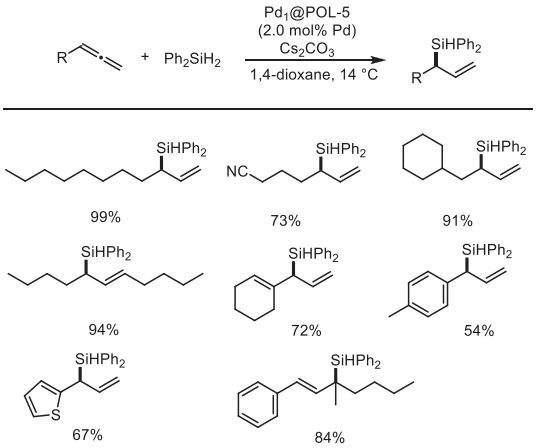


**Scheme 18.** Substrate scope for hydrosilylation of allenes with $Pd_1$@POL-5.

co-workers [86]. This catalyst can catalyze the stereoselective hydrosilylation of internal alkynes to give (*E*)-vinylsilanes in excellent yields. Then they developed other rhodium nanoparticles with controllable morphology and size, which were stabilized by nitrogen-rich polyoxyethylene derivatives [87]. These nanomaterials were prepared *via* the reduction of rhodium(III) chloride trihydrate with $NaBH_4$ in water at room temperature (Fig. 26). The flower-like Rh NPs were effective for the stereoselective hydrosilylation of internal alkynes to form (*E*)-vinylsilanes in excellent yields under solvent-free conditions. Specifically, the presence of water leads to the transfer hydrogenation products when using the Pd catalyst. This rhodium nanoparticle catalyst has good recyclability and is insensitive to the presence of water.

Porous organic polymers (POPs) have the character of high surface areas, good stabilities, and tunable pore size distribution. These insoluble porous polymers with catalytic sites adopted onto their framework can enhance the performance in catalysis. A $Co(acac)_2$/POL-$PPh_3$ catalyst was developed by Zhan and co-workers to catalyze (*E*)-selective hydrosilylation of alkynes with $PhSiH_3$ for the synthesis of (*E*)-$\beta$-vinylsilanes with high regio- and stereoselectivity [88]. This polymer-based cobalt catalyst could be recycled several times in a continuous flow system without loss of activity and selectivity. The heterogeneous earth-abundant cobalt catalyst for hydrosilylation shows potential industrial application.

In 2020, they developed another conjugated microporous polymer with pyridine units containing adjacent C≡C bonds. The resulting parts-per-million (ppm) levels catalyst (Pd–CMP-1) was a highly efficient catalyst for regioselective allene hydrosilylation to produce branched allylsilanes (Scheme 17) [89]. The catalyst was compatible with aliphatic allenes bearing various functional and reactive groups. The confinement effect of the porous structure of the polymer was beneficial for regioselectivity control.

Using trace amounts (<1 ppm) of metal catalysts in organic synthesis is rare and shows potential for industry application. Very recently, Zhan and co-workers designed and synthesized a single-atom Pd-based porous organic ligand polymer $Pd_1$@POL [90]. This catalyst can realize the hydrosilylation of allenes with 0.98 ppm Pd loading with regioselectivity > 100:1 (Scheme 18). This low Pd loading catalyst showed super catalytic efficiency for hydrosilylation of allene with turnover number up to 772,358, which was 200 times higher than previously reported. This catalyst could be recycled numerous times in a continuous flow system without any loss in activity and selectivity.

## 7. MOFs based catalyst

Metal-organic frameworks (MOFs) are prepared from organic ligands and metal nodes. They exhibit unique properties in many areas, including application in heterogeneous catalysis [91], such as degradation of organic pollutants [92], $CO_2$ utilization [93], hydrogenation reactions [94], oxidations [95].

MOFs based materials were also developed for the silylations of unsaturated bonds. In 2016, Lin *et al.* synthesized a new two-dimensional material MOLs using [$Hf_6(\mu_3\text{-}O)_4(\mu_3\text{-}OH)_4$(carboxylate)$_{12}$] and benzene-1,3,5-tribenzoate (BTB). Uniform MOLs with monolayer thickness can be obtained using a reactant molar ratio of $HfCl_4$/BTB/$HCO_2H$/$H_2O$/DMF = 1.5:1:830:290:2280 by heating the mixture at 120 °C for 48 h. Then the doping with 4′-(4-benzoate)-(2,2′,2′-terpyridine)-5,5′′-dicarboxylate (TPY) to coordinate with the iron center can lead to the MOL catalyst Fe-TPY-MOL (Fig. 27) [96]. Pure anti-Markovnikov product in 100% yield was obtained with 0.02% Fe-TPY-MOL for the hydrosilylation of styrene with $PhSiH_3$ (TON > 5000) (Scheme 19). Notably, no product was observed for the MOF with an interlocked 3D structure. The MOL-immobilized Fe-TPY species are true molecular catalysts by preventing bimolecular disproportionation.

Later, they report another example of a porous Zr-MOF based on a triarylphosphine-derived tricarboxylate linker. Single-site mono(phosphine)-Rh or Ir catalysts were obtained after metala-

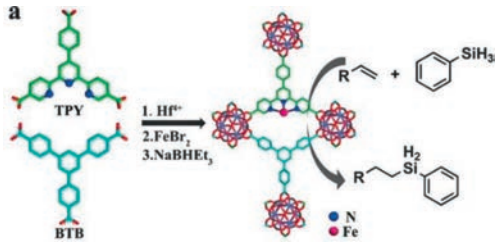


**Fig. 27.** MOLs loaded with Fe catalytic centers for the hydrosilylation of terminal olefins. Copied with permission [96]. Copyright 2016, John Wiley and Sons.

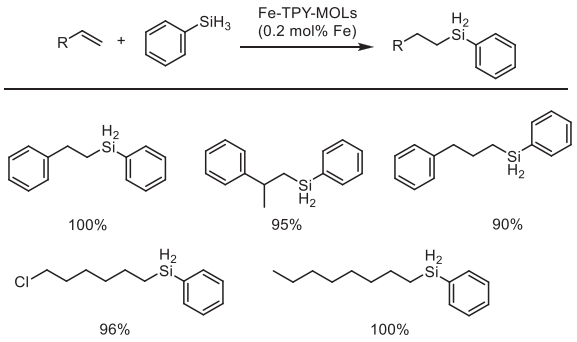


**Scheme 19.** Fe-TPY-MOL catalyzed the hydrosilylation of styrene with $PhSiH_3$.

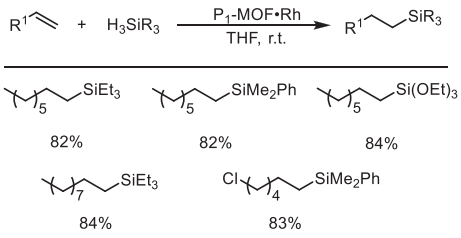


**Scheme 20.** Single-site mono(phosphine)-Rh catalyst for alkene hydrosilylation.

tion [97]. These catalysts show superior activity for the hydrosilylation of alkenes than a corresponding homogeneous catalyst (Scheme 20). For example, hydrosilylation of 1-octene with triethylsilane catalyzed by 0.0001 mol% catalyst at room temperature for 72 h can give the product in 82% yield (TON = 820,000). The MOF catalysts can also be reused multiple times without any loss of catalytic activity.

In 2019, Hu *et al.* developed a new nickel carboxylate MOFs, which can be easily prepared by mixing a nickel salt with dicarboxylic acid or polycarboxylic acid ligands [98]. These Ni MOF catalysts show excellent activity for anti-Markovnikov hydrosilylation of alkenes with turnover numbers up to 9500. The best catalyst can be reused for ten recycling runs without obvious activity loss. The substrate scope under this catalytic system is broad, with an excellent functional group tolerance (Scheme 21). Very recently, Peng and co-workers reported a Co-MOF for hydrosilylation of styrene or its derivatives with $Ph_2SiH_2$ in the presence of $NaBHEt_3$ [99]. A variety of linear alkenes and aromatic olefins can be converted to linear alkylsilanes with excellent activity and selectivity.

The hydrosilylation of multiple-functional alkenes with silanes can lead to a product with one or more functional groups for further transformation, especially substrates with two double bonds. However, the most popular Karstedt's catalyst usually leads to unisolable mixtures without good selectivity. Therefore, high site selectivity for hydrosilylation with a broad scope of substrates is still desired in industry production. Liu and co-workers reported a cage-trapped Pt catalyst (COP1-T-Pt) that exhibited very high activity and interesting size-selectivity for important alkoxysilanes synthesis from alkene hydrosilylations (Scheme 22) [100]. Due to the confined environment of cage-trapped Pt catalyst, it exhibited remarkable size selectivity and high site selectivity for alkenes with multiple functional groups. For example, only the allyl addition product was obtained for substrate allyl methacrylate due to the less steric hindrance, and no methacrylate addition product was detected.

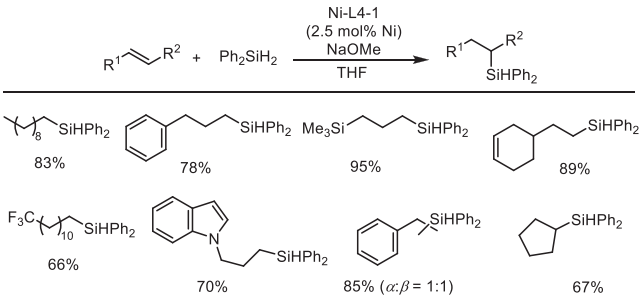


**Scheme 21.** Substrates scope of nickel carboxylate MOFs catalyzed alkene hydrosilylation.

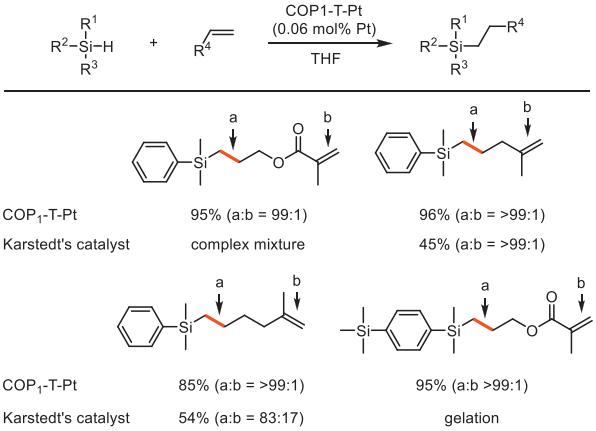


**Scheme 22.** Hydrosilylation with multiple functional substrates with site-selective effect.

## 8. Conclusion and outlook

We summarized the recent development of heterogeneous catalysts for unsaturated C-C bond hydrosilylations, including alkene, alkyne, and allene (Table 1). The progress in this area is of great interest for both academic and industrial investigations in that the silicone industry always desires new improvements in catalysis and technology. The present review discusses the heterogeneous hydrosilylation catalysts based on the following support: silicon, molecular sieve, carbon material, metal oxide, organic polymer, and MOFs material. The metal immobilization on these supports can form supported metal complexes, nanoparticles, or single-atom catalysts. Most of these catalysts show high hydrosilylation activities and selectivities with good recycling properties. For most case, terminal alkene and alkyne show high activity under the heterogeneous catalytic systems.

However, the comprehensive understanding of the original relationship between structural and the regio- and stereoselectivity is still urgent because this is important for the catalysts' rational design for further development.

Nevertheless, most of the reported heterogeneous catalysts are based on noble metals (Pt, Rh, Pd, Ru), although inexpensive non-noble metal based homogeneous catalysis has been well developed. The use of non-noble metals such as Fe, Ni, and Co for het-

**Table 1**
Summary of different catalysts for hydrosilylations.

| Catalyst | Substrate | Number of substrate | Yield (%) | TON/TOF | Ref. |
|---|---|---|---|---|---|
| Karstedt/$SiO_2$ | Styrene | 1 | 93 | | [23] |
| Rh/$SiO_2$ | Terminal alkene | 4 | 88-97 | | [24] |
| Rh/$SiO_2$ | Terminal alkene | 15 | 82-99 | | [25] |
| Rh/$SiO_2$ | Terminal alkene | 7 | 65-99 | | [26] |
| Rh-$NEt_2$/$SiO_2$ | Terminal alkene | 12 | 71-99 | | [27] |
| Rh-$NEt_2$/$SiO_2$ | Allylbenzene | 1 | 80 | | [28] |
| Rh/$SiO_2$/$Bu_3NI$ | Terminal alkene | 9 | 47-99 | | [29] |
| Rh-I-N/$SiO_2$ | Terminal alkene | 12 | 47-99 | | [30] |
| '$SiO_2$'-$NH_2$-Pt | Terminal alkene | 5 | 91-97 | | [31] |
| $SiO_2$-EDTA-Pt | 1-Hexene | 1 | 99 | | [32] |
| Pt/$SiO_2$ | Terminal alkene, internal alkene | 11 | 22-99 | | [33] |
| SiliaCat Pt(0) | Terminal alkene | 5 | 68-99 | | [35] |
| SiliaCat Pt(0) | Terminal alkene, terminal alkyne | 27 | 73-98 | | [36] |
| $Pd_1Cu_2$/$SiO_2$ | Terminal alkyne, internal alkyne | 22 | 87-99 | | [37] |
| Pt/MCM-41 | Terminal alkene | 7 | 63-94 | | [38] |
| Rh/MCM-41 | Terminal alkene | 7 | 71-93 | | [39] |
| Ru/MCM-41 | 1-Hexyne | 1 | 27.5 | | [40] |
| Ru/MCM-41 | 1–Hexyne | 1 | - | 2 (TON) | [41] |
| SBA-15-Naphth-Pt(COD) | Terminal alkene<br>Internal alkene | 9 | 23-99 | | [42] |
| Pt@{walls}SBA-15 | 1-Octene | 1 | - | $10^5$ (TON) | [43] |
| Pt/SBA-15 | Phenylacetylene | 1 | | | [44] |
| Pt/SBA-APTE-SA | Terminal alkene | 5 | 91-97 | | [45] |
| Pt/$SiO_2$/$Fe_3O_4$ | Allyl polyether | 1 | 87 | | [46] |
| $Fe_3O_4$@$SiO_2$-APTES-Pt | Terminal alkene | 6 | 61-98 | | [47] |
| Pt/vinyl/ $SiO_2$/$Fe_3O_4$ | Allyl polyether | 1 | 92 | | [48] |
| $Fe_3O_4$@$SiO_2$-BA@ Pt | Terminal alkene, internal alkene<br>Terminal alkyne, internal alkyne | 15 | 30-99 | | [49] |
| $Fe_3O_4$@$SiO_2$@Pt | Terminal alkene, internal alkene | 19 | 57-99 | | [50] |
| $Fe_3O_4$@$SiO_2$-biIMI-$PtCl_2$ | Terminal alkene, internal alkene | 10 | 18-99 | | [51] |
| Rh or Pt on MgO-$SiO_2$ and MgO-$SiO_2$/lignin supports | 1-Octene | 1 | 2-99 | | [52] |
| [$PtMe_2$(BPyPMO-TMS)] | Phenylacetylene | 1 | 98 | | [53] |
| GO-Karstedt | Terminal alkene | 6 | 78-93 | | [55] |
| Pt/GNP | Terminal alkene | 15 | 33-99 | | [56] |
| Pt-ISA/NG | Terminal alkene | 15 | 92-99 | | [57] |
| nano-PtNi/NC | 1-octene | 1 | 99 | | [58] |
| Pt/rGO | Terminal alkyne, internal alkyne | 7 | 87-99 | | [59] |
| $PtFe_3$/CN | Terminal alkene | 13 | 96-99 | | [60] |
| Rh/TRGO | Terminal alkyne | 7 | 96-99 | | [61] |
| PtCNT | Terminal alkene, internal alkene<br>Terminal alkyne, internal alkyne | 23 | 91-99 | | [62] |
| $Au_1$/g-$C_3N_4$ | Terminal alkyne | 12 | 85-99 | | [63] |
| Pt–MgO and Ru–MgO | Terminal alkyne | 3 | 99 | | [64] |
| Au/C and Au/$\gamma$-$Al_2O_3$ | Terminal alkyne | 3 | 34-83 and 81-99 | | [65] |
| Au/$CeO_2$ | Terminal alkene | 3 | 100 | | [67] |
| Au/$TiO_2$ | Terminal alkyne | 19 | 74-94 | | [68] |
| $PtO_2$ | Terminal alkene | 12 | 85-95 | | [69] |
| $PtO_2$ | 1-Octene | 1 | - | 95000 (TOF/$h^{-1}$) | [70] |
| Pt/$TiO_2$ | Terminal alkyne, internal alkyne | 16 | 88-98 | | [71] |
| Pt/NR-$Al_2O_3$-IP | Terminal alkene | 32 | 57-97 | | [72] |
| 1Pd5Au/$Al_2O_3$ | Allene | 15 | 21-79 | | [73] |
| $Pt_1^{\delta+}$/$TiO_2$ | 1-Octene | 1 | - | 780 (TOF/$h^{-1}$) | [74] |
| Pt-DPTZ/MgO | 1-Octene | 1 | 96 | | [75] |
| Pt/$CeO_2$ | 1-Octene | 1 | 90 | | [76] |
| Pt-DPTZ/$TiO_2$ | 1-Octene | 1 | 97 | | [77] |
| Rh/$CeO_2$ + Ru/$CeO_2$ | Internal alkene | 7 | 37-83 | | [78] |
| $Ru^{\delta+}$/$ZrO_2$ | Ethylene | 2 | 96-99 | | [79] |
| Co/$TiO_2$ | Terminal alkene | 12 | 80-93 | | [80] |
| $Fe_2O_3$ NPs | Terminal alkene | 13 | 39-84 | | [81] |
| xPSt–SH–Pt | Terminal alkene | 5 | 25-83 | | [82] |
| Pt/poly(styrene-*co*-chloromethylstyrene) | Vinylsilanes | 1 | 100 | | [83] |
| Pt/copolymer | 3,3,3-Trifluoropropene | 1 | 93 | | [84] |
| Pt/PEG-AMB | Terminal alkene | 14 | 24-98 | | [85] |
| Pd/tris-imidazolium-tetrafluoroborates | Internal alkyne | 18 | 60-99 | | [86] |
| Rh/PEG | Internal alkyne | 24 | 69-99 | | [87] |
| Co/POL-$PPh_3$ | Terminal alkyne | 31 | 42-93 | | [88] |
| Pd/CMP-1 | Allene | 39 | 50-94 | | [89] |
| $Pd_1$/POL-5 | Allene | 20 | 54-99 | | [90] |
| Fe-TPY-MOLs | Terminal alkene | 7 | 85-100 | | [96] |
| Rh/$P_1$-MOF | Terminal alkene | 5 | 82-84 | | [97] |
| Ni/MOFs | Terminal alkene, internal alkene | 29 | 53-95 | | [98] |
| Co/MOF | Terminal alkene | 12 | 61-99 | | [99] |
| Pt/COP1-T | Terminal alkene | 19 | 60-97 | | [100] |

erogeneous catalyst exploration, especially for industrial production, is still desired but challenging.

## Declaration of competing interest

The authors declare that they have no known competing financial interests or personal relationships that could have appeared to influence the work reported in this paper.

## Acknowledgments

We are grateful for the financial support from the National Natural Science Foundation of China (No. 22001227), the Natural Science Foundation of Jiangsu Province (No. BK20200919), the "Jiangsu Specially-Appointed Professor Plan", and the Priority Academic Program Development of Jiangsu Higher Education Institutions.

## Supplementary materials

Supplementary material associated with this article can be found, in the online version, at doi:10.1016/j.cclet.2023.109257.

## Reference

[1] B. Marciniec, Hydrosilylation: A Comprehensive Review on Recent Advances, Springer Science, 2009.
[2] E. Rémond, C. Martin, J. Martinez, F. Cavelier, Chem. Rev. 116 (2016) 11654–11684.
[3] R. Ramesh, D.S. Reddy, J. Med. Chem. 61 (2018) 3779–3798.
[4] L. Li, Y.L. Wei, L.W. Xu, Synlett 31 (2020) 21–34.
[5] F. Ye, Z. Xu, L.W. Xu, Acc. Chem. Res. 54 (2021) 452–470.
[6] F. Ye, L.W. Xu, Synlett 32 (2021) 1281–1288.
[7] L.X.W. Huang, Chin. J. Org. Chem. 41 (2021) 4515–4516.
[8] H. Wang, X. Zhang, Y. Li, L.W. Xu, Angew. Chem. Int. Ed. 61 (2022) e202210851.
[9] X. Zhang, J. Fang, C. Cai, G. Lu, Chin. Chem. Lett. 32 (2021) 1280–1292.
[10] L.H. Sommer, E.W. Pietrusza, F.C. Whitmore, J. Am. Chem. Soc. 69 (1947) 188-188.
[11] J.L. Speier, J.A. Webster, G.H. Barnes, J. Am. Chem. Soc. 79 (1957) 974–979.
[12] B. Karstedt, Patent: US3775452A, 1973.
[13] L.D. de Almeida, H. Wang, K. Junge, X. Cui, M. Beller, Angew. Chem. Int. Ed. 60 (2021) 550–565.
[14] P.F. Fu, L. Brard, Y. Li, T.J. Marks, J. Am. Chem. Soc. 117 (1995) 7157–7168.
[15] K. Takaki, K. Sonoda, T. Kousaka, et al., Tetrahedron Lett. 42 (2001) 9211–9214.
[16] J. Li, C. Zhao, J. Liu, et al., Inorg. Chem. 55 (2016) 9105–9111.
[17] D.S. Levine, T.D. Tilley, R.A. Andersen, Chem. Commun. 53 (2017) 11881–11884.
[18] J. Liu, W. Chen, J. Li, C. Cui, ACS Catal. 8 (2018) 2230–2235.
[19] X. Liu, Q. Wen, L. Xiang, X. Leng, Y. Chen, Chem. Eur. J. 26 (2020) 5494–5499.
[20] W. Chen, H. Song, J. Li, C. Cui, Angew. Chem. Int. Ed. 59 (2020) 2365–2369.
[21] W. Chen, C. Jiang, J. Zhang, et al., J. Am. Chem. Soc. 143 (2021) 12913–12918.
[22] S. Zhu, W. Xu, D. Hong, et al., Inorg. Chem. 62 (2023) 381–391.
[23] Q.J. Miao, Z.P. Fang, G.P. Cai, Catal. Commun. 4 (2003) 637–639.
[24] B. Marciniec, K. Szubert, M.J. Potrzebowski, I. Kownacki, K. Łęszczak, Angew. Chem. Int. Ed. 47 (2008) 541–544.
[25] B. Marciniec, K. Szubert, R. Fiedorow, et al., J. Mol. Catal. A: Chem. 310 (2009) 9–16.
[26] B. Marciniec, K. Szubert, M.J. Potrzebowski, I. Kownacki, H. Maciejewski, ChemCatChem 1 (2009) 304–310.
[27] K. Motokura, K. Maeda, W.J. Chun, ACS Catal. 7 (2017) 4637–4641.
[28] K. Maeda, Y. Uemura, M. Kim, et al., J. Phy. Chem. C 123 (2019) 14556–14563.
[29] K. Usui, K. Miyashita, K. Maeda, et al., Org. Lett. 21 (2019) 9372–9376.
[30] K. Usui, Y. Manaka, W.J. Chun, K. Motokura, Chem. Eur. J. 28 (2022) e202104001.
[31] J. Li, C. Yang, L. Zhang, T. Ma, J. Organomet. Chem. 696 (2011) 1845–1849.
[32] F. Li, Y. Li, J. Mol. Catal. A: Chem. 420 (2016) 254–263.
[33] D. Shao, Y. Li, RSC Adv. 8 (2018) 20379–20393.
[34] A.J. Chalk, J.F. Harrod, J. Am. Chem. Soc. 87 (1965) 16–21.
[35] R. Ciriminna, V. Pandarus, G. Gingras, F. Béland, M. Pagliaro, ACS Sustain. Chem. Eng. 1 (2013) 249–253.
[36] V. Pandarus, R. Ciriminna, G. Gingras, et al., Green Chem. 21 (2019) 129–140.
[37] J.W. Zhang, G.P. Lu, C. Cai, Green Chem. 19 (2017) 2535–2540.
[38] R. Hu, L. Zha, M. Cai, Catal. Commun. 11 (2010) 563–566.
[39] R. Hu, W. Hao, M. Cai, Chin. J. Chem. 29 (2011) 1629–1634.
[40] D. Do Van, T. Hosokawa, M. Saito, Y. Horiuchi, M. Matsuoka, Appl. Catal. A: Gen. 503 (2015) 203–208.
[41] D. Van Do, T. Hosokawa, Y. Horiuchi, M. Matsuoka, Res. Chem. Interm. 46 (2020) 5297–5306.
[42] Y. Huo, J. Hu, S. Lin, et al., Appl. Organomet. Chem. 33 (2019) e4874.
[43] T. Galeandro-Diamant, R. Sayah, M.L. Zanota, et al., Chem. Commun. 53 (2017) 2962–2965.
[44] D.G. Dobó, D. Sipos, A. Sápi, et al., Catalysts 8 (2018) 22.
[45] W. Chen, Z. Xie, H. Liang, et al., RSC Adv. 10 (2020) 3175–3183.
[46] H. Zai, Y. Zhao, S. Chen, et al., RSC Adv. 6 (2016) 98520–98527.
[47] J. Zhao, Y. Gui, Y. Liu, et al., Catal. Lett. 147 (2017) 1127–1132.
[48] H. Zai, Y. Zhao, S. Chen, et al., Nano Res. 11 (2018) 2544–2552.
[49] L. Li, Y. Li, A. Assefa, J.J. Bao, Transit. Metal Chem. 44 (2019) 779–787.
[50] L. Li, Y. Li, J. Yan, et al., RSC Adv. 9 (2019) 12696–12709.
[51] Y. Huo, J. Hu, Y. Tu, et al., J. Organomet. Chem. 936 (2021) 121714.
[52] O. Bartlewicz, M. Zieliński, M. Kaczmarek, H. Maciejewski, Mol. Catal. 509 (2021) 111615.
[53] Y. Naganawa, Y. Maegawa, H. Guo, et al., Dalton Trans. 48 (2019) 5534–5540.
[54] Y. Zhu, S. Murali, W. Cai, et al., Adv. Mater. 22 (2010) 3906–3924.
[55] F. Rao, S. Deng, C. Chen, N. Zhang, Catal. Commun. 46 (2014) 1–5.
[56] C.J. Kong, S.E. Gilliland, B.R. Clark, B.F. Gupton, Chem. Commun. 54 (2018) 13343–13346.
[57] Y. Zhu, T. Cao, C. Cao, et al., ACS Catal. 8 (2018) 10004–10011.
[58] J. Wen, Y. Chen, S. Ji, et al., Nano Res. 12 (2019) 2584–2588.
[59] A. Mollar-Cuni, P. Borja, S. Martin, G. Guisado-Barrios, J.A. Mata, Eur. J. Inorg. Chem. 2020 (2020) 4254–4262.
[60] Y. Han, Y. Xiong, C. Liu, et al., J. Catal. 396 (2021) 351–359.
[61] B. Sánchez-Page, M.V. Jiménez, J.J. Pérez-Torrente, et al., ACS Appl. Nano Mater. 3 (2020) 1640–1655.
[62] D.V. Jawale, V. Geertsen, F. Miserque, et al., Green Chem. 23 (2021) 815–820.
[63] X. Feng, J. Guo, S. Wang, Q. Wu, Z. Chen, J. Mater. Chem. A 9 (2021) 17885–17892.
[64] R. Jiménez, J.M. López, J. Cervantes, Can. J. Chem. 78 (2000) 1491–1495.
[65] A.M. Caporusso, L.A. Aronica, E. Schiavi, et al., J. Organomet. Chem. 690 (2005) 1063–1066.
[66] S. Carrettin, P. Concepción, A. Corma, J.M. López Nieto, V.F. Puntes, Angew. Chem. Int. Ed. 43 (2004) 2538–2540.
[67] A. Corma, C. Gonzalez-Arellano, M. Iglesias, F. Sanchez, Angew. Chem. Int. Ed. 46 (2007) 7820–7822.
[68] A. Psyllaki, I.N. Lykakis, M. Stratakis, Tetrahedron 68 (2012) 8724–8731.
[69] N. Sabourault, G. Mignani, A. Wagner, C. Mioskowski, Org. Lett. 4 (2002) 2117–2119.
[70] S. Putzien, E. Louis, O. Nuyken, F.E. Kühn, Catal. Sci. Technol. 2 (2012) 725–729.
[71] F. Alonso, R. Buitrago, Y. Moglie, et al., J. Organomet. Chem. 696 (2011) 368–372.
[72] X. Cui, K. Junge, X. Dai, et al., ACS Cent. Sci. 3 (2017) 580–585.
[73] H. Miura, S. Sasaki, R. Ogawa, T. Shishido, Eur. J. Org. Chem. 2018 (2018) 1858–1862.
[74] Y. Chen, S. Ji, W. Sun, et al., J. Am. Chem. Soc. 140 (2018) 7407–7410.
[75] L. Chen, G.E. Sterbinsky, S.L. Tait, J. Catal. 365 (2018) 303–312.
[76] L. Chen, I.S. Ali, S.L. Tait, ChemCatChem 12 (2020) 3576–3584.
[77] X. Zhou, L. Chen, G.E. Sterbinsky, et al., Catal. Sci. Technol. 10 (2020) 3353–3365.
[78] B.B. Sarma, J. Kim, J. Amsler, et al., Angew. Chem. Int. Ed. 59 (2020) 5806–5815.
[79] M. Li, S. Zhao, J. Li, et al., Nano Res. 15 (2022) 5857–5864.
[80] T. Mitsudome, S. Fujita, M. Sheng, et al., Green Chem. 21 (2019) 4566–4570.
[81] R. Azuma, S. Nakamichi, J. Kimura, et al., ChemCatChem 10 (2018) 2378–2382.
[82] C. Kan, X. Kong, C. Du, D. Liu, Polym. J. 34 (2002) 97–102.
[83] A. Kowalewska, J. Organomet. Chem. 693 (2008) 2193–2199.
[84] Y. Bai, J. Peng, Y. Hu, J. Li, G. Lai, J. Fluorine Chem. 132 (2011) 123–127.
[85] Y. Bai, S. Zhang, Y. Deng, et al., J. Colloid Interface Sci. 394 (2013) 428–433.
[86] M. Planellas, W. Guo, F. Alonso, et al., Adv. Syn. Catal. 356 (2014) 179–188.
[87] W. Guo, R. Pleixats, A. Shafir, T. Parella, Adv. Syn. Catal. 357 (2015) 89–99.
[88] R.H. Li, X.M. An, Y. Yang, et al., Org. Lett. 20 (2018) 5023–5026.
[89] Y.N. Jiang, J.H. Zeng, Y. Yang, et al., Chem. Commun. 56 (2020) 1597–1600.
[90] L. Pang, X. Li, S.C. Ren, et al., Nano Res. 15 (2022) 7091–7098.
[91] A. Bavykina, N. Kolobov, I.S. Khan, et al., Chem. Rev. 120 (2020) 8468–8535.
[92] T. Xia, Y. Lin, W. Li, M. Ju, Chin. Chem. Lett. 32 (2021) 2975–2984.
[93] C.A. Trickett, A. Helal, B.A. Al-Maythalony, et al., Nat. Rev. Mater. 2 (2017) 17045.
[94] Q. Shen, X. Li, R. Li, Y. Wu, ACS Sustain. Chem. Eng. 8 (2020) 17608–17621.
[95] A. Dhakshinamoorthy, A.M. Asiri, H. Garcia, Chem. Eur. J. 22 (2016) 8012–8024.
[96] L. Cao, Z. Lin, F. Peng, et al., Angew. Chem. Int. Ed. 55 (2016) 4962–4966.
[97] T. Sawano, Z. Lin, D. Boures, et al., J. Am. Chem. Soc. 138 (2016) 9783–9786.
[98] Z. Zhang, L. Bai, X. Hu, Chem. Sci. 10 (2019) 3791–3795.
[99] Z. Yu, Z. Song, C. Lu, et al., Appl. Organomet. Chem. 36 (2022) e6648.
[100] G. Pan, C. Hu, S. Hong, et al., Nat. Commun. 12 (2021) 64.